CENTRO DE INVESTIGACIONES EN ÓPTICA, A.C.

Study on abatement of insertion losses in the mechanical cleave of POF through: thermal polish and controlled temperature cleave

Final version. Includes changes suggested by advisors.

MASTER IN OPTOMECHATRONICS

Assessor:

PhD. Ismael Torres Gómez

Student:

Engr. Francisco Javier Vargas Muñoz

March 2017
León, Guanajuato, México

Blank page.

Preface

In 2014, Mexico is located in the 7th place of the global market of automotive producers, representing the 3% of the national Gross Domestic Product (GDP) [1]. Mexico is expected to produce more automotive parts than Korea or Germany by the year 2020.

In the state of Guanajuato, OEM automotive manufacturers have been established: Mazda, Honda, General Motors, Volkswagen, Toyota, Hino and Ford.

Guanajuato automotive corridor.

Components as cables, wires and harness are needed in the automotive supply chain. Today's automotive networks require a flexible medium of communication, which can support high transmission rates at low cost. Polymer Optical Fibers (POF) satisfy the requirements for in-vehicle data transmission.

The company Arneses Electricos Automotrices, S.A. de C.V. (ARELA), part of the Condumex group, supply the automotive market. This company

[1] Source: ProMexico 2017

previously studied the use of POF cables in the automotive industry, with applications according to the Media Orientated System Transport (MOST) standard.

Low losses POF cables are typically generated trough procedures which involves several steps. This work proposes optimal conditions to generate POF cables that meets the automotive standards with minimum steps. Furthermore, it can be used as a previous version of the automation process for the manufacture of POF cables.

Several end face terminations methods are exposed in this work, with a focus on those related to increasing temperature. Every termination method attenuation is measured following the standard TIA-526-14-B, corresponding to the multimode fiber attenuation measurement method. Finally, a comparison of termination methods available for POF cables is conducted.

On Chapter 1, the major properties of polymer optical fibers are reviewed, and compared to those of silica fibers. Chapter 2 discuss the polymer optical fibers in the automotive industry. A brief description of in-vehicle communication networks is presented, with a focus on the MOST system. Chapter 3 shows the planning of the conducted experiments, which are centered to increasing temperature termination process. Chapter 4 presents the results of the described experiments. Afterwards these results are compared to a reference.

Acknowledgment

The author wants to express gratitude to CONACYT for the scholarship support. To the Centro de Investigaciones en Optica, which improved my professional formation. The under-all-circumstances helpful fiber optics group.

Special thanks to PhD. Yuri Barmenkov and PhD. Armando García Villegas for their opportune comments on this work. Also, sincere thanks to PhD. Ismael Torres Gómez for his tireless guidance.

To all of my professors, thanks for the pressure and their knowledge. To all my colleagues, thanks for the shared moments.

To my family, thanks for being there. Plus Ultra.

Resume

Stimulated from the recently regional automotive growth, the automobile industry have implemented optical communications as a fast, reliable and inexpensive data communication system. Automobile networks requires a flexible medium of transmission that can support high data rates at low costs. Plastic optical fibers (POFs) are suitable for this purpose.

This work exposes several termination methods used for plastic optical fibers, orientated to heating methods. Methods as hot blade cleaving, increase of the fiber's temperature and hot plate are presented. The objective of these terminations methods is to reduce the losses originated from the POF end face surface, thus achieving an efficient, low attenuation POF cable. The usage of POFs in automobile network systems is reviewed. Finally, a comparison between typical termination techniques, as polishing, and heating methods is realized. The results obtained could serve as a scope for a future POF cable automation process.

Table of Acronyms

Acronym	Name
AMP	Amplifier
ARP	Address Resolution Protocol
CAI	Cavity As Interface
CAN	Controller Area Network
CD	Compact Disc
D2B	Digital Domestic Bus
DAB	Digital Audio Broadcast
DSP	Digital Signal Processor
DVD	Digital Video Disc
ECU	Electronic Control Unit
EMI	Electtromagnetic Interference
ePhy	Electrical physical (layer)
ETFE	Ethylene Tetrefluoroethylene
FOT	Fiber Optic Transceiver
FWHM	Full Width at Half Maximum
GI	Graded Index
GSM	Global System for Mobile Communications
IDB 1394	Intelligent Data Bus 1394
IP	Internet Protocol
IPX	Internetwork Packet Exchange
LED	Light Emitting Diode
LIN	Local Interconnect Network
LS	Light source
MOST	Media Orientated System Transport
NA	numerical aperture
NAVI	Navigation system
NetBEUI	NetBIOS Extended User Interface
NI	National Instruments
NIC	Network Interface Controller
oPhy	Optical physical (layer)
PA-12	Polyamide 12
PC	Personal Computer
PCI	Peripheral Component Interconnect
PCS	Polymer Cladded Silica
PF - GI	Perfluorinated Graded Index

Continued*

Acronym	Name
PM	Power Meter
PMMA	polymethyl methacrylate
PMMA - d_8	deuterated PMMA
POF	Plastic Optial Fiber
Ps	Polystyrene
PXI	PCI eXtensions for Instrumentation
rms	root mean square
SI	Step Index
SP	Specification Point
TCP/IP	Transmission Control Protocol/ Internet Protocol
TIR	Total Internal Reflection
TTA	Time Triggered Architechture
TTL	Transistor Transistor Logic
TTP/C	Time Triggered protocol
TV	Television
UTP	Unshielded Twisted Pair (of cables)

Study on abatement of insertion losses in the mechanical cleave of POF through: thermal polish and controlled temperature cleave

Francisco Javier Vargas Muñoz

March 2017

Contents

1 Plastic Optical Fiber (POF): Optical transmission properties and applications

In general, optical fibers are waveguides used in the optical communications field. Commonly, the term optical fiber is directly associated to glass. The market domination of glass fibers displaces Polymer Optical Fibers (POFs) to the background, even when POFs predate glass fibers. Nowdays POFs are reaching larger markets with improved technology and applications. The history of POF can be recorded as an series of efforts to decrease the transmission loss. Table 1 presents some of the major advances related to the POF.

Year	Development
1968	Dupont company develops PMMA fiber.
1990	Professor Koike reports the manufacture of graded index polymer optical fiber.
1995	Keio University and KAIST group presented fluoropolymer fiber.
1998	MOST cooperation founded.
2001	First MOST built in car presented

Table 1: Brief evolution of the POF advances. Adapted from Ref. [A2] PMMA, polymethyl methacrylate, MOST, Media Orientated System Transport

In the early 1960s, POFs with polymethacrylates were originated by Pilot Chemical of Boston. Their developments passed to Dupont, which presented the PMMA fiber in 1968. Years later, in 1978 Mitsubishi Rayon company acquired Dupont. Afterwards, Mitsubishi was able to diminish the loss of POF fibers close to the theoretical limit. In 1990, the group directed by Prof. Koike reported a manufacture process for graded index POFs. Later, in 1995 Prof. Koike and his colleges developed a graded index POF with perfluorinated polymer, which posses losses below non perfluorinated POFs. By 2001, the first MOST built in car was commercially introduced [A1]. Today POFs developments are orientated (but not restricted) to data communication [A2].

1.1 Plastic Optical Fiber structure

The structure of a Polymer Optical Fiber is described in Figure 1. The fiber core, with a diameter of 980 μm, is composed by polymethyl methacrylate (PMMA); and the cladding, with an outer diameter of 1000 μm, which is made of a fluorinated polymer. Following the manufacturer's specifications, the typical values for the core and cladding refractive index, correspond to $n_1 = 1.492$ and $n_2 = 1.405$ respectively. In addition, the typical numerical aperture (NA) magnitude is 0.5. The operational temperature limit is + 85 °C [A3].

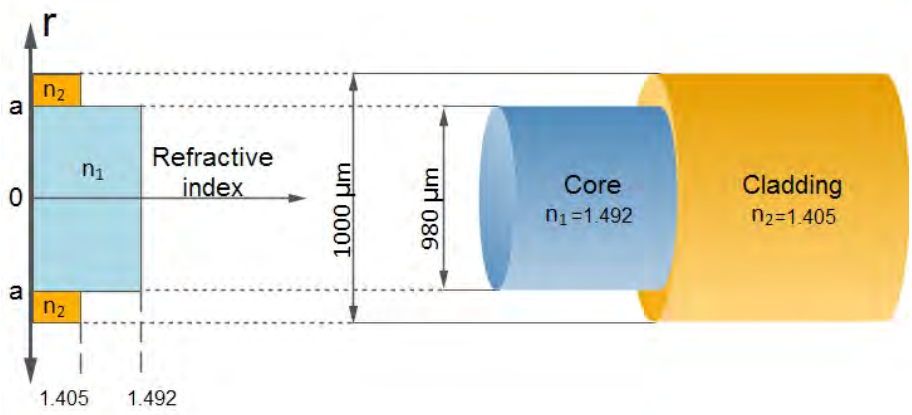

Figure 1: PMMA POF structure and typical values. Not to scale.

Due to physical-chemical properties, as transition temperature, tensile strength and water susceptibility, polymethyl methacrylate (PMMA) is mostly used as the core in the commercial fabrication of POF [A4]. Besides PMMA, deuterated PMMA (PMMA - d_8) posses lower attenuation with the same properties of the PMMA.

In applications where high temperature is required, materials as polycarbonate (PC) or Zeonex® are used in the core of POF. Topas® is a POF core alternative with matching properties of Zeonex®. Polystyrene (PS) is mainly used in side emitting POF, and also is widely used for ornamental POF. CYTOP® is primary used in small core graded index plastic fibers, with low transmission loss [A5].

The standard POF posses a core / cladding diameter of 980 μm / 1000

μm. Additionally, various core / cladding diameters are available for others POFs (Table 2).

Fiber type	Core diameter	Cladding diameter
Perfluorinated Graded Index (PF-GI) POF	120 μm	500 μm
Graded Index (GI) POF.	500 μm	750 μm

Table 2: Various core / cladding diameters of POF.

The propagation of light through a medium other than vacuum result in a reduction of light speed. The refractive index, n, is defined as the ratio of the speed of light in the vacuum c_0, and the speed of light in the medium c_m. This is expressed as:

$$n = c_0/c_m \tag{1}$$

As the core and the cladding are composed by different materials, both posses diverse refractive index, n_1 for the core and n_2 for the cladding.

The numerical aperture NA, represent the capacity of an optical fiber to gather and confine light from an optical source due to total internal reflection (TIR). A common expression for NA is:

$$NA = \sqrt{n_1^2 - n_2^2} \tag{2}$$

In a step index profile (SI), the values of the core and cladding refractive index remains constants through the entire cross section. According to Figure 2, a SI profile fiber is defined as:

$$\begin{array}{c} n_1 = n_{core} \quad \text{if} \quad r \leq a \\ n_2 = n_{clad} \quad \text{if} \quad r > a \end{array} \tag{3}$$

Where a represents the radius of the core. Due to the large core of POFs and therefore its significant NA, the amount of modes traveling are in the order of millions. Individual rays travels different distances, thus, differences in the transit time causes the original signal to broadens [A6].

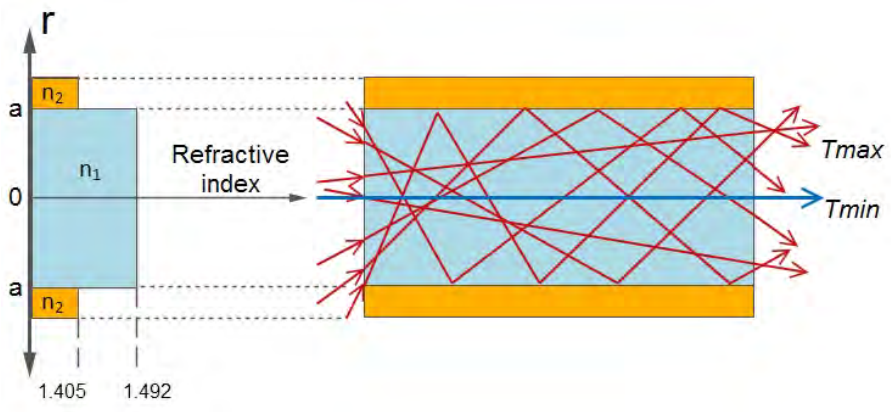

Figure 2: Ray trace propagation and index profile in a step index POF.

Because different modes posses different optical paths, parameters as propagation and absorption are mode dependent. Further information is available in section 1.2 of this chapter. Figure 13 shows the field distribution of a POF; where launching light with a small angle concentrates the modes to the center of the waveguide.

1.2 Attenuation mechanisms

Transmission loss

In a general manner, the Beer-Lambert Law relates the light attenuation between the input and the output of a propagation medium. The attenuation coefficient (α) represents the loss per unit length in the fiber, where both absorption and scattering are included. The loss in decibels, in a specific length (L) of fiber is defined as:

$$T_{dB} = \alpha L \tag{4}$$

The optical power transmitted through a fiber can be expressed as:

$$T = \left(\frac{P_{out}}{P_{in}} \right) \tag{5}$$

Where P_{out} and P_{in} correspond to the optical power at the output and the input of the fiber system respectively. The fraction of the optical power

transmitted through the fiber is rewritten in decibels as [A7]:

$$T_{dB} = 10\log(T) = 10\log\left(\frac{P_{out}}{P_{in}}\right) \tag{6}$$

Basically, the transmission loss limits the distance a signal can propagate until that signal degrades and the optical power becomes undetectable. Transmission loss measures, the light loss between the input and the output of an optical component (optical fiber). It includes the sum of all losses [A8].

Attenuation is wavelength and material dependent. The mechanisms involved in the contributions of POF losses are fundamentally similar to those of silica fibers, but with different magnitudes. These mechanisms are pointed in Figure 3.

Two main categories describe the attenuation factors in POF: Intrinsic Losses originated from the fiber's material, and the Extrinsic Losses, which appear from impurities and imperfections in the fiber's fabrication.

Besides the mentioned loss mechanisms, parameters as coupling loss, mechanical stress, bending, climate changes, dispersion and fiber aging also increment the fiber losses. The most relevant parameters are reviewed in Chapter 3 of this work.

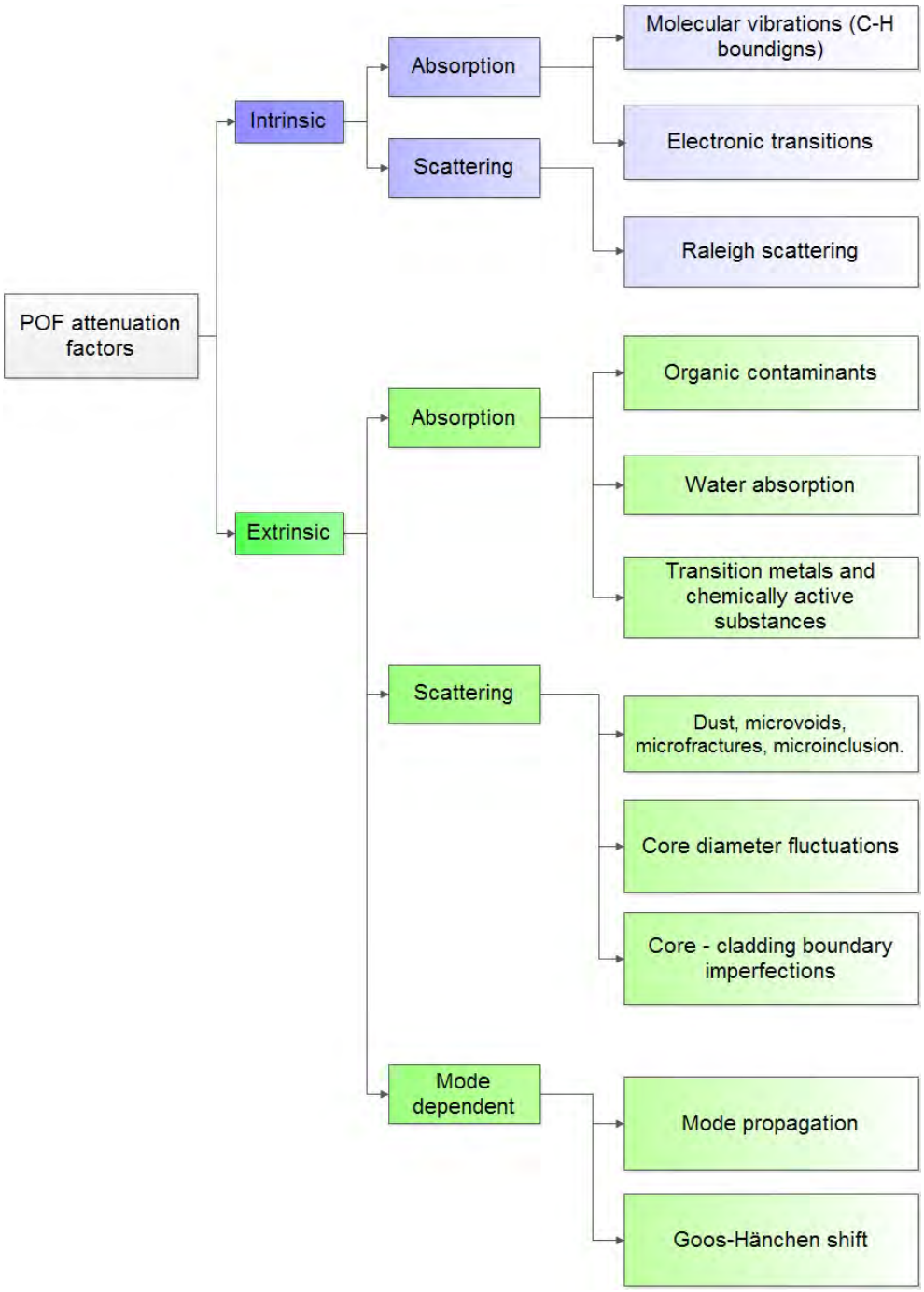

Figure 3: Major attenuation factors of POF.

Intrinsic losses

Intrinsic losses are related with the fiber's material composition. Mechanisms of absorption from molecular vibrations, electronic transitions and Rayleigh scattering originate these losses.

Electronic transition absorption

An electronic transition appear when electrons in a lower energy level absorb light in the form of photons, thus the exited electrons move to higher energy levels. This transition causes absorption peaks usually in UV wavelengths, and occasionally in the visible spectrum. The absorption tails originated produce attenuation in the operational wavelength.

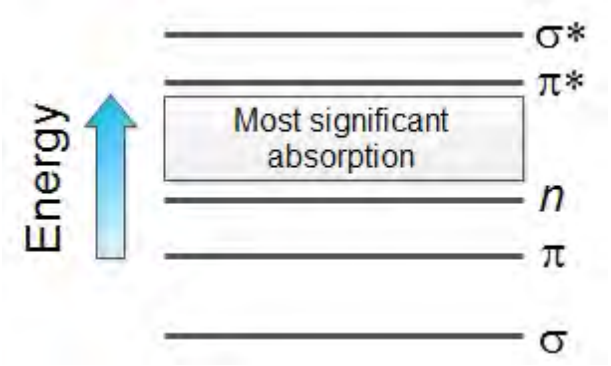

Figure 4: Energy levels for electrons. Adapted from Ref. [A9].

The major absorption appears in the n-π^* orbital transition, from the double bound in the ester group (Figure 4). According to the Urbach's rule, the electronic transition absorption posses exponential tails, expressed as:

$$\alpha_e = A \exp\left(\frac{B}{\lambda}\right) \tag{7}$$

Therefore, α_e represents the electronic transition absorption loss (dB/km), λ the incident wavelength (nm), and A and B values are 1.58 x10^{-12} and 1.15 x10^4 for the PMMA respectively.

Molecular vibration absorption

Absorption from the molecular vibrations is typically found in the infrared

spectrum, at wavelengths which correspond to the resonance frequency of fundamental molecular vibrations. Originated from IR higher harmonics, organic molecules absorb IR radiation and convert it into energy in the form of molecular vibrations.
Overtone and absorption bands arise in the near IR and visible spectrum. The stretching overtone absorption of the C-H bound provides the major molecular vibration absorption in POFs. The carbon-hydrogen bound act as a mass on a spring, therefore, light absorption occur at specific frequencies and the corresponding harmonics. Increasing the wavelength also increases the molecular absorption loss. [A4]

To reduce the C-H bound stretching absorption, the hydrogen atoms can be replaced by heavier elements as: deuterium, fluorine or chlorine and, theoretically, for any halogen element or rare earth. Thus, the molecular vibrations shifts towards greater wavelengths.

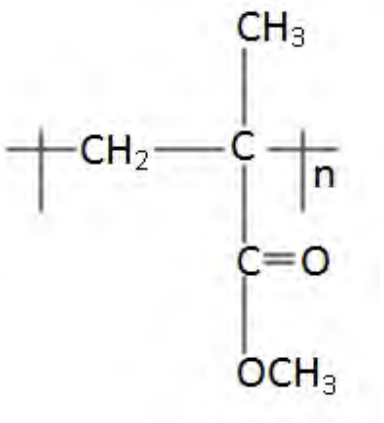

Figure 5: PMMA molecular structure. Adapted from Ref. [A9].

Rayleigh scattering
The Rayleigh scattering is originated from random changes in density, molecular structure and molecular orientation of the polymer. When the light propagates through the fiber, reflections and refractions occur, therefore the incident ray is scattered in all directions. According to the material, Rayleigh scattering is enhanced in shorter wavelengths. The irregularities that produces Rayleigh scattering posses a size of 1/10 of wavelength. An useful approximation of the Rayleigh scattering is:

$$\alpha_R \approx \frac{1}{\lambda^4} \tag{8}$$

Where λ indicates the incident wavelength. From the last equation is inquired that increasing the wavelength reduces the Rayleigh scattering loss. An expression of the Rayleigh attenuation specifically for PMMA POF is [A10]:

$$\alpha_R(PMMA) = 13\left(\frac{633}{\lambda}\right)^4 \tag{9}$$

Extrinsic losses

Extrinsic losses are related to imperfections and impurities in the fiber's core. Impurities as organic contaminants, water and transition metals produce light absorption, whereas imperfections, dust, bubbles and inclusions in the core - cladding boundary result in light scattering.
External environmental stress factors originate new imperfections and enlarge the effect of existing ones. Therefore, the fiber could suffer of premature aging.

Impurities absorption

The major extrinsic absorption correspond to transition metals and water. On the other hand, metal contaminants feature absorption bands in the visible and near IR spectrum. Cobalt ions represent the primary increase in attenuation; with a concentration of 2 ppb, losses of 10 dB/km arise (Table 3). This metal absorbs at 520 nm, 590 nm and 650 nm [A9]. Transition metals contributions could be in polymerization of preform using metal reactor and/or in manufacture process, mainly when extrusion is used.

Table 3: Loss induced by contaminants

Metal ion	Concentration ppm	Loss dB km^{-1}	Wavelength nm
Co	2	10	visible
Cr	1	1	650
Fe	1	0.7	1100
Cu	1	0.4	850
OH^-	1	50	1380
		2.4	1130
		1	950

Adapted from Ref [A10]. ppb indicates 1 impurity atom per 10^9 atoms.

Light absorption is augmented by organic contaminants as initiators and chain transfer agents. Resulting from the POF water absorption, the OH bound produces light absorption at the IR region. The influence of the OH vibrational absorption depends on the spectral location of the absorption; nevertheless peaks due to the hydroxyl group are commonly found in the infrared region. In PMMA based POF, the water is concentrated in the fiber's matrix, causing the fiber to swell.

Scattering due to imperfections
During the process of manufacture, alterations in the core and cladding contributes with imperfections as dust particles, inclusions, fractures, and air bubbles. These alteration produce light scattering, which is independent from the operational wavelength.

PMMA Loss factors summary

For simplification and representation of the terms described, the Table 4 represents the typical loss factors for PMMA polymer optical fiber, and Figure 6 indicates the percentage of loss of the same factors.

Theoretical loss limits of PMMA based optical fiber are pointed in Table 5, as well as its loss percentage in Figure 7.

Table 4: Loss factors at different wavelengths for PMMA POF.

Wavelength	nm	516	568	650
Absorption	dB km^{-1}	11	17	95
Rayleigh scattering	dB km^{-1}	26	18	10
Structural imperfection	dB km^{-1}	-	20	-
Total loss	dB km^{-1}	37	55	105

Adapted from Ref [A10].

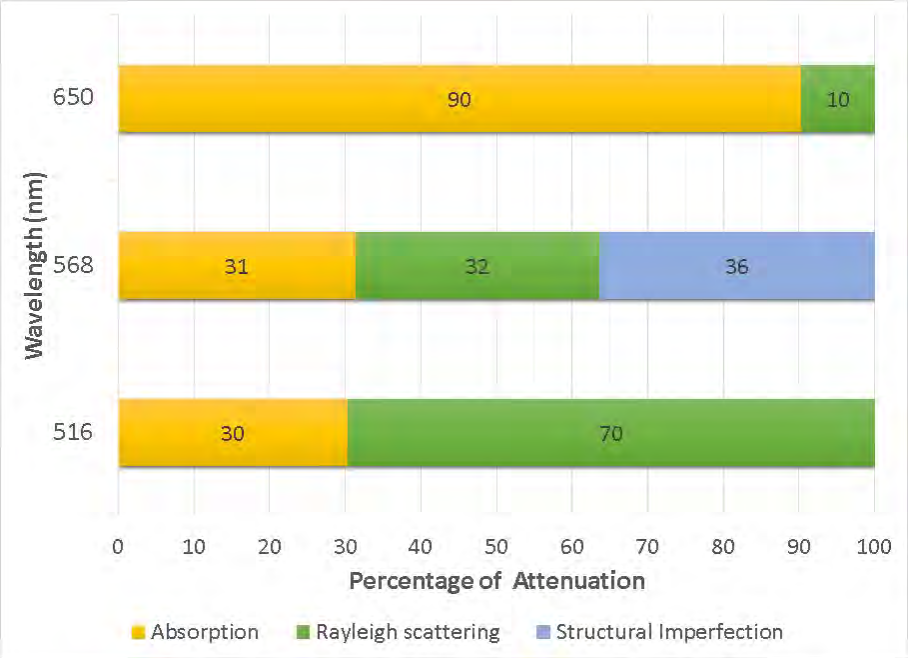

Figure 6: Percentage representation of PMMA loss factors at different wavelengths.

Table 5: Theoretical attenuation limits of PMMA POF.

Wavelength	nm	520	570	650
Rayleigh scattering	dB km^{-1}	28	20	12
UV absorption	dB km^{-1}	0	0	0
C-H absorption	dB km^{-1}	1	7	88
Total loss	dB km^{-1}	29	27	100

Adapted from Ref [A6].

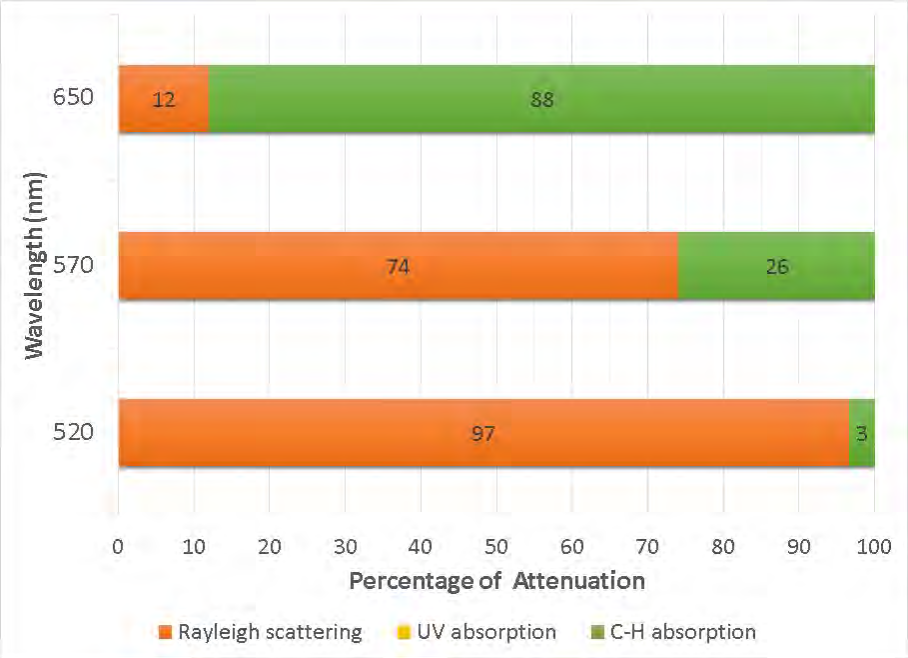

Figure 7: Percentage representation of theoretical limit of PMMA POF at different wavelengths.

Mode dependent attenuation

POFs possess mode dependent attenuation. The loss due to mode dependency increase for the highest modes. Lower modes have lower attenuation than higher modes. Diverse reasons explain this behavior: higher modes carry more intensity in the core-cladding boundary inducing

evanescence effects.

During the total internal reflection (TIR), the Goos-Hänchen shift appears. In every reflection in the core-cladding interface, light rays invade the cladding. The amount of light entering the cladding depending of the angle of incidence is expressed by:

$$\overline{\alpha}_{GH} = \frac{d_{GH}(\theta)}{a} \frac{\alpha_{clad}}{\cos(\theta)} \tag{10}$$

Where a correspond to the radius of the core, α_{clad} to the cladding material attenuation, θ to the angle of incidence, λ to the wavelength and $d_{GH}(\theta)$ represent the invasion depth in function of the angle of incidence, given by: [A6]

$$d_{GH}(\theta) = \frac{\lambda}{2\pi\sqrt{n_{core}^2 \cos^2(\theta) - n_{clad}^2}} \tag{11}$$

PMMA POF attenuation windows

Due to small changes in the fabrication process, the locations of the optical windows for PMMA posses minor variations.

	Green	Yellow	Red	Reference
Wavelength (nm)	520	560	650	[A11]
	516	568	650	[A12]

The wavelength of 650 nm, which is common, corresponds not only to the Media Orientated System Transport (MOST) peak wavelength, but also to the majority of the communications systems which are actually developed for short distance PMMA POF based communications.

Under and above this peak, the PMMA attenuation rises, thus, the optical specification for the MOST physical layer indicates a range from 630 to 685 nm and therefore, the width of the spectrum in the source is restricted to 30 nm at Full Width Half Maximum (FWHM) [A1]. The Figure 8 represents the attenuations windows and loss factors for PMMA.

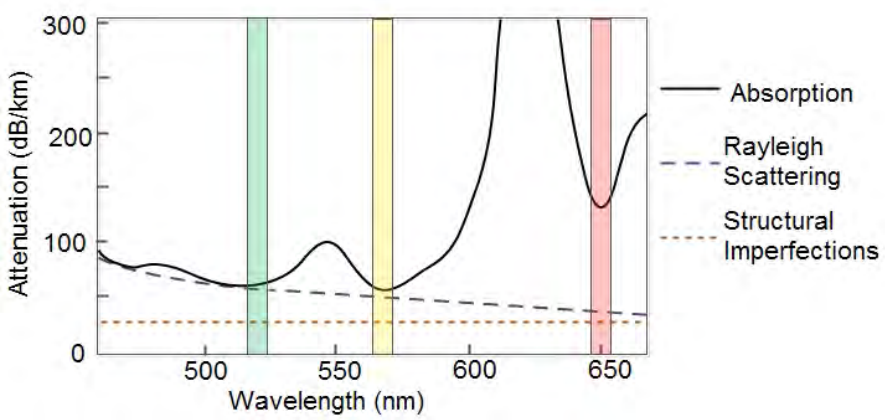

Figure 8: Attenuations windows and loss factors for PMMA POF. Adapted from Ref. [A12].

1.3 Dispersion

Fundamentally, dispersion is referred to every mechanism that produce a difference of the transit time in a transmission medium. In fiber optics, two major contributions result in pulse dispersion: different rays have diverse propagation time (intermodal dispersion), and different wavelengths transit at different times through an specific material (intramodal dispersion)[A13]. An overview of the principal dispersion mechanisms is detailed in section 1.3 of this work.

In multimode fibers, the major source of dispersion comes from intermodal dispersion. Different ray lights propagates in different paths through the fiber. Ray lights with less reflections (low order modes) travel shorter distances than rays that propagate in longer distances (high order modes). Therefore, low order modes arrive sooner to the receiver than high order modes.

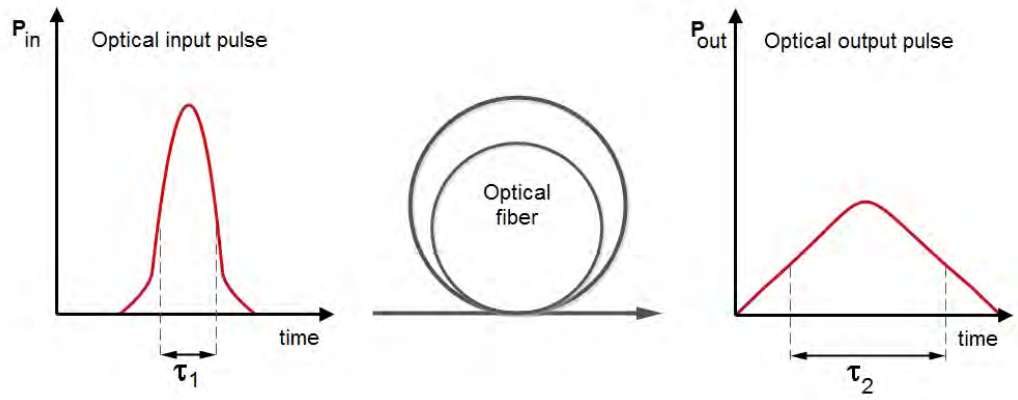

Figure 9: Pulse broadening while propagated. The width at the input $\tau_1 < \tau_2$ at the output.

The optical output pulse is composed by the merge of individual pulses. Each individual pulse posses a delay time respect each other, thus the optical output pulse is wider than the input pulse (Figure 9). An expression of this time interval is:

$$\Delta t = L\frac{n_1}{c}\left(\frac{n_1 - n_2}{n_2}\right) = L\frac{n_1}{c}\Delta \tag{12}$$

Where L is the length of the optical fiber and c is the speed of light. Δ is also known as the *relative refractive index*. In order to obtain an expression of dispersion per unit length (ns/km), the last equation is rewritten as [A14]:

$$\frac{\Delta t}{L} = \frac{n_1\Delta}{c} \tag{13}$$

When two adjacent pulses are propagated through an optical fiber, at certain point, the pulse contrast decreases, the broadening of the pulse enlarge, the adjacent pulses will overlap until the pulses can not be separated from each other and the output may not be resolvable by the receiver [A15]. This process is shown in Figure 10, where the pulse is modified from time t1 through time t4. At time t4, the pulses are unresolvable.

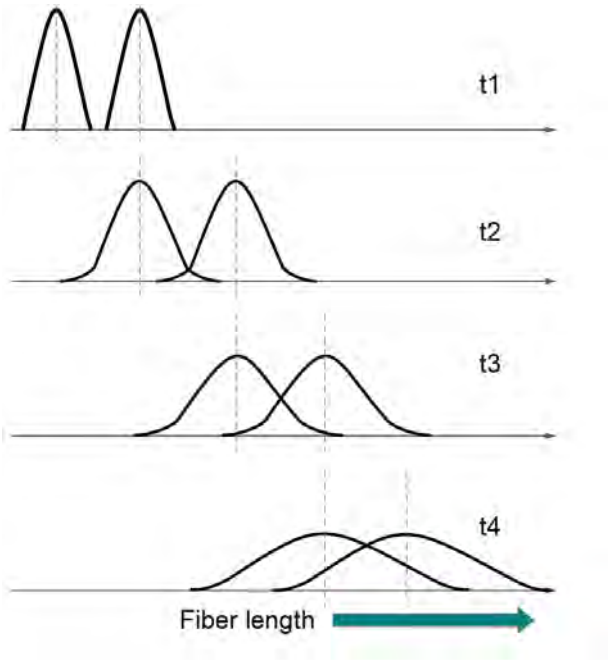

Figure 10: Overlapping and broadening of two pulses while propagated through an optical fiber.

This behavior is expected in high data rates and longer transmissions distances. The transmission bandwidth, the data transmission rate and the pulse minimum separation is limited by the pulse broadening. Therefore, the bandwidth decreases while increasing transmission distances. More detailed information of step index POFs bandwidht is available in section 1.3.

Dispersion mechanisms

As previously mentioned, two distortion mechanism cause the pulse broadening. Intermodal and intramodal dispersion.

The root mean squared (rms) width of the impulse response σ is calculated as:

$$\sigma = \sqrt{\sigma_{inter}^2 + \sigma_{intra}^2} \tag{14}$$

With σ_{inter} and σ_{intra} as the rms width of the pulse broadening for intermodal and intramodal dispersion respectively. Effects of the polarization mode dispersion can be neglected in multimode fibers. [A8]

Intermodal dispersion.
The intermodal dispersion, or modal dispersion, is referred as the pulse broadening effect when modes, initially launched at the same time, arrive at the output with a time delay. Different modes travel at different times along the fiber; therefore the input pulse will suffer a broadening.

The intermodal dispersion results as the variation in the group velocities of the different modes. Also can be referred as the difference between the travel time of the longest ray path T_{max} and the travel time of the shortest ray path T_{min} (Figure 2). This is expressed as [A16]:

$$\sigma_{inter} = T_{max} - T_{min} = \Delta t \tag{15}$$

Intramodal dispersion.
Defined as the broadening of the pulse which occurs within a single mode. The two causes of intramodal dispersion are: Material dispersion and Waveguide dispersion.

- Material dispersion
  Appears due to the changes of the refractive index of the core material as a function of the wavelength, provoking a wavelength dependence of a given mode.

  $$\sigma_{mat} = L\Delta\lambda \frac{\lambda}{c} \frac{\mathrm{d}^2 n(\lambda)}{\mathrm{d}\lambda^2} = L\Delta\lambda M(\lambda) \tag{16}$$

  Where $\Delta\lambda$ is the spectral width of the transmitter, $n(\lambda)$ the wavelength dependent refractive index, and $M(\lambda)$ are the material dispersion parameters. [A6]

  Material dispersion is usually expressed in ps/nm·km. Figure 11 represents the material dispersion of Silica glass, Perfluorinated (PF) polymer and PMMA.

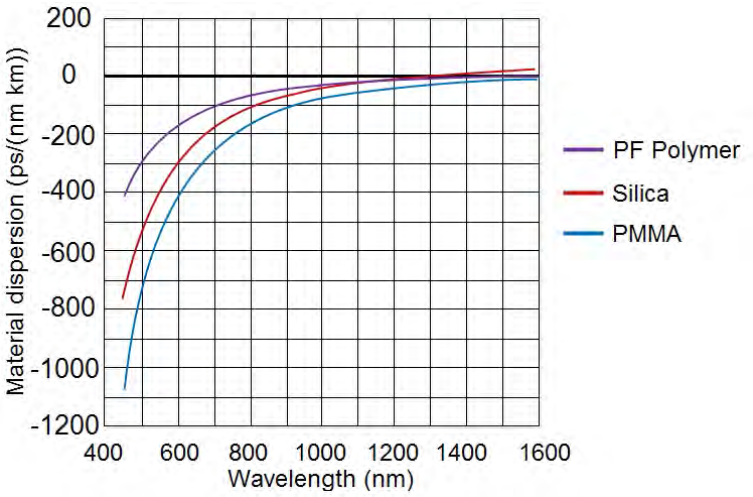

Figure 11: Comparison of material dispersion. Adapted from Ref. [A17].

In common applications of optical fibers, the negative value indicates that while increasing the wavelength, the time delay diminishes, thus a greater transmission speed can be achieved.

- Waveguide dispersion
  It appears from the wavelength dependence of the optical confinement of a mode between the core and the cladding. Light at shorter wavelength is more confined in the core, whereas with longer wavelengths the light is concentrated closer to the cladding. Waveguide dispersion is usually ignored in multimode fibers.

Bandwidth of step index POF

For short distances, a step index POF has no changes in bandwidth while variating the diameter. Nevertheless, a reduction in diameter results in a decrease of reflections. These reflections affects modal process as mode attenuation and mode coupling. Figure 12 relates the bandwidth, and length with various POF diameters.

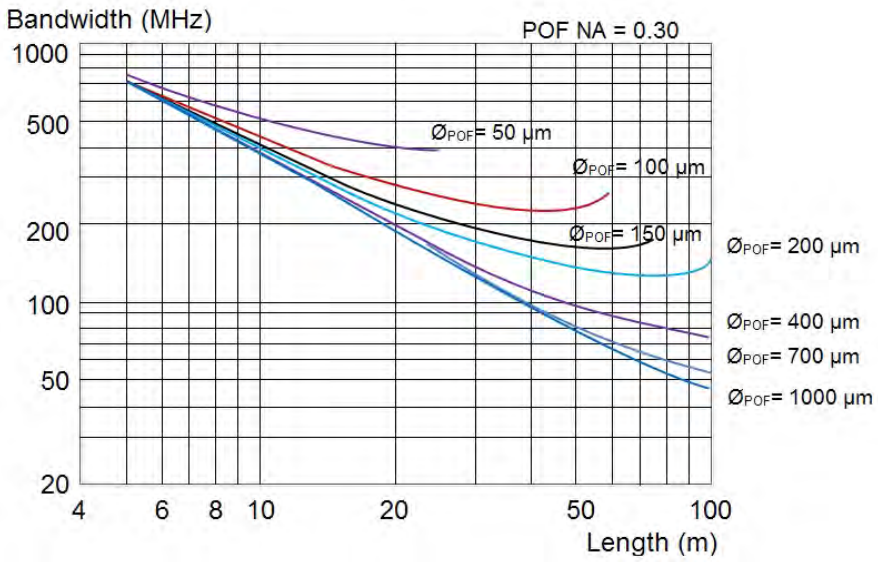

Figure 12: Theoretical Bandwidth with diverse POF core diameters. Adapted from Ref. [A6].

In addition of the bandwidth change, the optical power propagation is affected by modal processes, as millions of modes travel along the fiber. Figure 13 represents the far field distribution of a 50 μm diameter POF. At 20 m, the far field has decreased its width by half, causing an bandwidth increase of 400%. Because of the fact that different modes posses different optical paths (Figure 2); launching light with a small angle concentrates the modes to the center of the waveguide. Thus, an adequate bandwidth with acceptable losses is generated.

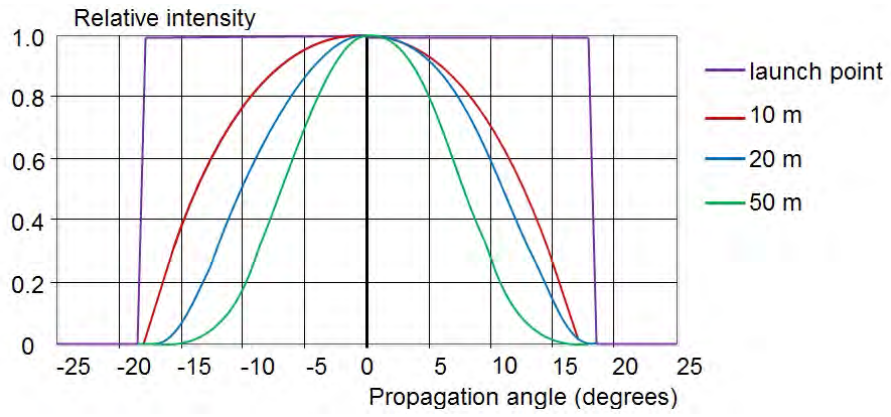

Figure 13: Simulations of far field distribution of 50 μm diameter POF. Adapted from Ref. [A6].

1.4 POF vs glass fiber

POFs used in data communication offer advantages and disadvantages when compared with communication grade silica optical fiber. Table 6 indicates an overview of these advantages and disadvantages.

In comparison, the connectors, couples and housings are less expensive than those designed for the silica based fiber optic. The dimensional magnitudes and tolerances used in POFs are greater; resulting in a low priced manufacture. Also, the large core of the POF provides relative immunity to dust; minor contamination will not inevitably break the optical transmission. [A15]

Silica fiber	**Polymer Optical Fiber**
SiO_2 core	PMMA core
Light weight	Light weight
Low flexibility	High flexibility
Easy handling and positioning	Careful handling and precise positioning needed
Protection against electromagnetic interference (EMI)	Protection against electromagnetic interference (EMI)
Operation in the infra red spectrum	Operation in the visible spectrum
Eye protection recommended	Intrinsic eye security
Required specialized training	Do it yourself requirements
Inefficient light coupling due to low NA	Efficient light coupling due to high NA
Low losses	High losses
Appropriate for transmission distances of kilometers	Not suitable for transmission distances over 100 m
Suitable for temperatures above 85 °C	Operational temperature limited to 85°C
Several developments available	Few developments present
Well known standards	Few published standards
Large number of suppliers	Few suppliers available

Table 6: Comparison between POF and silica based fibers used in data transmission

POF mechanical properties

Principal mechanical properties of large core PMMA polymer optical fiber used in the conducted experiments, are presented in Table 7. A more detailed version of this table is available in Appendix 1 of this work.

Element	Property	Symbol	Units	Value
PMMA	Core diameter	ϕ_{pmma}	μm	980
	Young's Modulus	E	MPa	3850
	Tensile strength	σ_t	MPa	85
	Poisson ratio	ν		0.34
PA-12	Inner jacket diameter	ϕ_{pa12}	μm	1510
	Young's Modulus	E	MPa	1450
	Tensile strength	σ_t	MPa	60.5
	Poisson ratio	ν		0.35
SiO_2	Core diameter	ϕ_{Si}	μm	8.2
	Young's Modulus	E	MPa	70608
	Tensile strength	σ_t	MPa	4903
	Poisson ratio	ν		0.17

Table 7: Comparison of mechanical material properties used in POFs and silica fibers.

1.5 Applications of POF

In a general manner, the applications of POF are divided into two groups: data transmission and non data communication. The Functionality of the data transmission group is clearly data communication between an emitter and a receiver. On the other hand, the group of non data communication includes systems which covers sensors, signs, illumination and others.[A2].

The data communication group is limited in distance, being 100 meters (or less) a reasonable limit for data link POF. Besides the receiver and the emitter, it is needed cables, connector and housings. Specifically in the automotive industries, by the year 2001, the maximum POF link length reported was 20 meters [A18].

Over the past decade, a POF *breakthrough application* in the automotive industry has impulsed new developments on this area. The characteristics of the POF solve the automotive needs of illumination and communication. The trends indicate a transition to an optical based in-vehicle network. Further information is available in Chapter 2 of this work.

1.6 Chapter 1 Conclusions

- Large core polymer optical fibers are multimode fibers limited in temperature and operational distance, but improved in handling and inexpensive materials when compared to silica based optical fibers.

- Pulse broadening is caused by Intermodal (mode) dispersion and Intramodal dispersion. Material dispersion is the primary cause of the Intramodal dispersion. The dispersion which posses a wavelength dependency sometimes is called chromatic dispersion.

- Mechanisms which causes losses in silica based optical fibers are fundamentally similar to those of polymer based optical fibers, but with different magnitude.

- Due to improved characteristics over other mediums, POF posses breakthrough applications in illumination and data transmission in the automotive industry.

1.7

Chapter 1 References

[A1] Andreas Grzemba. *MOST: The automotive multimedia network; from MOST25 to MOST150.* Franzis Verlag GmbH, 2011.

[A2] Paul Polishuk. Plastic optical fibers branch out. *IEEE Communications Magazine*, 44(9):140–148, 2006.

[A3] Mitsubishi. Eska Polymer Optical Fiber. Technical report, Mitsubishi Rayon Co., Ltd., Tokyo, 2016. `http://www.pofeska.com`.

[A4] N Ioannides, E B Chunga, A Bachmatiuk, I G Gonzalez-Martinez, B Trzebicka, D B Adebimpe, D Kalymnios, and M H Rümmeli. Approaches to mitigate polymer-core loss in plastic optical fibers: a review. *Materials Research Express*, 1(3):032002, 2014.

[A5] Markus Beckers, Tobias Schlüter, Thomas Vad, Thomas Gries, and Christian Alexander Bunge. An overview on fabrication methods for polymer optical fibers. *Polymer International*, 64(1):25–36, 2015.

[A6] Olaf Ziemann, Jürgen Krauser, Peter E. Zamzow, and Werner Daum. *POF Handbook Optical Short Range Transmission Systems.* Springer Berlin Heidelberg, Berlin, Heidelberg, 2008.

[A7] J Downing. *Fiber Optic Communications,.* Cengage Learning, 2004.

[A8] Y. Koike. *Fundamentals of Plastic Optical Fibers.* Wiley-VCH Verlag GmbH & Co. KGaA, Weinheim, Germany, dec 2014.

[A9] P Harmon Julie. Polymers for Optical Fibers and Waveguides: An Overview. *Optical Polymers*, pages 1–23, 2001.

[A10] Joseba Zubia and Jon Arrue. Plastic Optical Fibers: An Introduction to Their Technological Processes and Applications. *Optical Fiber Technology*, 7(2):101–140, 2001.

[A11] Mohamed Atef and Horst Zimmermann. *Optical Communication over Plastic Optical Fibers*, volume 172 of *Springer Series in Optical Sciences.* Springer Berlin Heidelberg, Berlin, Heidelberg, 2013.

[A12] Toshikuni Kaino. Preparation of plastic optical fibers for near-IR region transmission. *Journal of Polymer Science Part A: Polymer Chemistry*, 25(1):37–46, jan 1987.

[A13] Ajoy Ghatak and K. Thyagarajan. *Introduction to fiber optics*. Cambridge University Press, Cambridge, 1998.

[A14] Djafar K. Mynbaev and Lowell L. Schneiner. *Fiber-optic communications technology*. Prentice-Hall, 1st edition, 2001.

[A15] Andreas Weinert. *Plastic Optical Fibers: principles, components, installation*. Publicis MCD Verlag, Berlin, 1999.

[A16] G Keiser. *Optical fiber communication*. MGH International Editions, Singapore, second edition, 1991.

[A17] Yasuhiro Koike. Progress of plastic optical fiber technology. *Optical Communication, 1996. ECOC'96. 22nd European Conference on*, 1:41–48, 1996.

[A18] Eberhard Zeeb. Optical Data Bus Systems in Cars : Current Status and Future Challenges. *Proceedings 27th Erupean Conference on Optical Communications*, pages 70–71, 2001.

2 POF in the automotive industry

2.1 Automotive control and communication system evolution

Electrical networks

In the initial generations of automotive electronics, a stand alone electronic control unit (ECU) was implemented for each operation where the driver needed assistance in the control of the vehicle, such as steering, braking and traction. The ECU acts as a subsystem, and it is composed of a micro controller, sensors and actuators. Afterwards, in the beginning of 1990s, production vehicles were equipped with communication networks for ECU modules, the data reception and transmission was conducted by point to point links between ECUs. The last method of communication requires a number of channels of n^2, where n applies for the number of ECUs [B1].

Later in the same decade, research departments of vehicle brands produced approaches to use systems of **steer by wire** or **break by wire** in mass production models. Electronic control units, with sensors and actuators manage data with high availability [B2].

The **X by wire** technology execute functions related to the steering or braking. The term refers to the replacement of mechanical or hydraulic systems with electric or electronics systems.

In 1991 Bosch developed the Controller Area Network (**CAN bus**) as the first bus system introduced in mass production. By today, it is the most used network in the automotive industry [B3].

The **Flexray** bus was developed in 2000 by the consortium formed from BMW, Daimler Chrysler, Philips and Freescale [B4].

Optical networks

The use of POF networks in automotive systems begun when in 1997, Daimler Chrysler introduced the Digital Domestic Bus **D2B** on Mercedes

Benz cars. Using a ring topology, the D2B system communicates the telematics with infotainment equipments [B5].

In 1998, the Media Orientated Systems Transport **MOST** cooperation was founded by the group formed by BMW, Daimler Benz, Becker and OASIS Silicon Systems. With a ring topology, the MOST system interconnects different multimedia devices between each other. By today, more than 200 premium vehicles posses this network architecture.

In 2001, BMW developed an optical data bus for the airbags systems, called **byteflight**. This system uses a point to point network, and interconnects with a central active star coupler.

The data bus systems **D2B**, **MOST** and **byteflight** uses basically the same optical and electro-optical components. A large numeric aperture PMMA core POF as the waveguide, 650 nm LED as sources and large areas silicon based photoreceivers [B6]. In Figure 14, the evolution of the POF in automotive applications is illustrated.

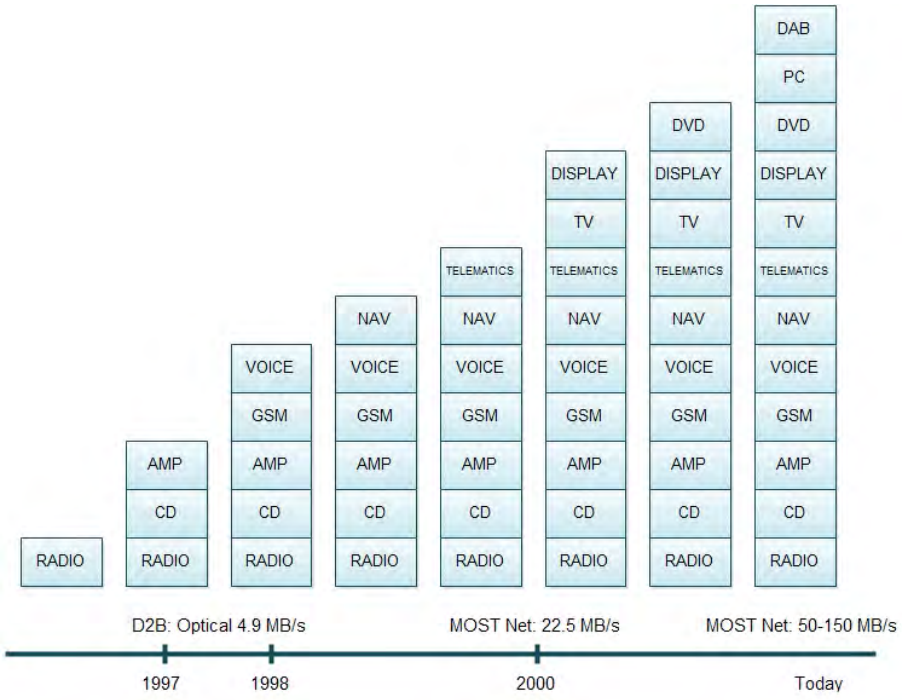

Figure 14: Development of optical networks in cars. Adapted from Ref. [B7]. Compact Disc (CD), Amplifier (AMP), Global System for Mobile communication (GSM), Navigation systems (NAVI), Television (TV), Digital Video Disc (DVD), Personal Computer (PC), Digital Audio Broadcast (DAB).

2.2 POF used in the infotainment automotive network

Polymer optical fibers (POF) consist of a polymer core and a lower index polymer cladding. In short distance data transmission, as well as illumination, fibers with polymethyl methacrylate (PMMA) core and fluorinated polymer cladding are commonly used. The characteristics of the POF make them perfectly suitable for applications in the automotive industry.

The key characteristics of the POF include:

- Improved flexibility
- High numerical aperture
- Lightweight
- Large core diameter
- Low cost

POF fibers are mainly limited by temperature. Due to material properties, PMMA core POF operate in the range of -40 °C to +85 °C [B8]. Places where the temperature increases above 85 °C, as the engine or the exhaust system, are not suitable for this type of fibers.

The D2B system, used particularly in Mercedes Benz cars, served as basis for the MOST system. Thus, dimensions and materials of both systems are almost equal. Figure 15. Core, cladding and jacket materials for both systems are polymethyl methacrylate (PMMA), Fluorinated polymer and Polyamide 12 (PA 12), respectively. PA 12 material is used for the fixation between the ferrule and the POF cable, when the fixation process is performed by laser welding.

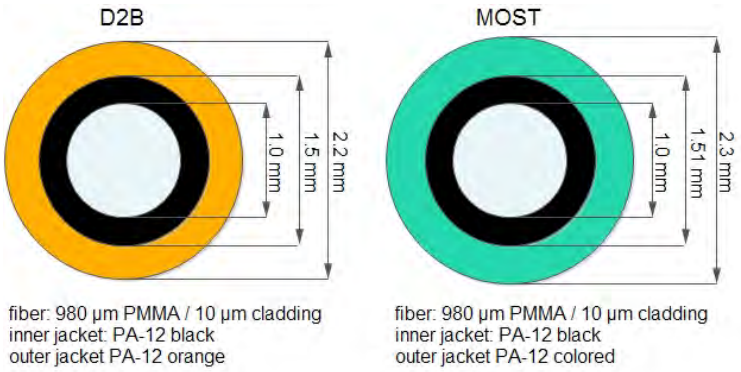

Figure 15: POF comparison between D2B and MOST. Not to scale.

Polymer Cladded Silica fibers

In harsh or high temperature environments, polymer cladded silica (PCS)

fibers serve as an alternative for POF. Due to the core material, these fibers are not strictly POFs. PCS fibers posses a silica core and a fluorinated polymer cladding. The buffer material is commonly made of ethylene tetrafluoroethylen (ETFE). In the jacket, materials as polyamide, polyolefin, or thermoplastic elastomer are used (Figure 16).

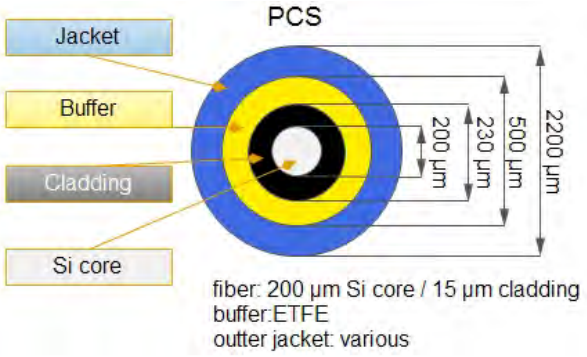

Figure 16: General dimensions of Polymer Cladded Silica (PCS) fiber. Not to scale.

The silica core provides different characteristics to the PCS fibers. Compared with POF and D2B fibers, in the range of $\lambda = 600$ nm to 900 nm, PCS fibers posses a lower optical attenuation of under 1 dB. Also, the operational temperature for the PCS fibers is up to 125 °C [B9].

2.3 CAN network

CAN Overview

The Controller Area Network (CAN) was developed as a high integrity multi master serial bus which communicates with other CAN nodes. Each device connected to the CAN network posses a CAN network node.

CAN network nodes are capable of receive and transmit data through the bus line. These nodes are composed by a CAN controller and a CAN transceiver. Each CAN node evaluates the incoming signal and, if necessary, forwards it to the required location. Thus, every device in the network acquire the transmitted data. Network nodes deliver and share information

between ECUs.

This network is the worldwide most used in-vehicle network. Also, became an ISO standard in 1994 (ISO 11898:1993). By today, the latest CAN ISO standard published is ISO 11898-2:2016 for high speed medium access unit.

The CAN posses advantages as:

- Good price / performance ratio.
- Low development cost.
- Reliable data transmission.
- Error detection capability.
- Real time application.

Different to others point-to-point networks, the CAN broadcast short messages through the complete network. CAN systems support data transmission up to 1 Mb/s. Commonly, the electronic control units (ECU) have a single CAN interface to every device in the system. Reducing importantly the number of harness and wires in vehicles.

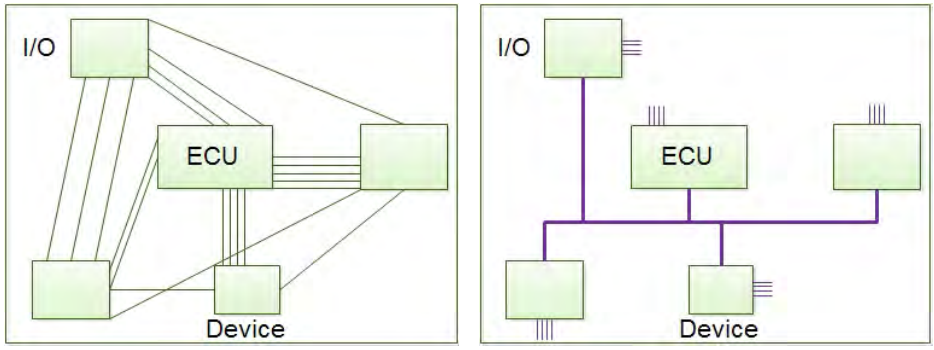

(a) Without CAN. (b) With CAN.

Figure 17: CAN wire reduction. Input / Output (I/O). Adapted from Ref. [B10].

CAN physical layer

Even when the standard defines a single line of twisted pair network topology (Bus topology), active star CAN topology is also available. In the bus topology, to minimize reflection on the electrical signal, each end of the bus lines posses a 120 Ω resistance. Figure 18.

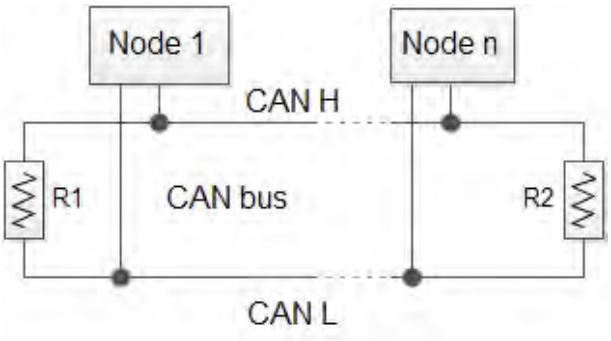

Figure 18: CAN bit transmission bus lines.

Single wire line and two wire line are possible for the CAN system. In the single wire line, all bus nodes share a common ground, which works as the second line.

In the other case, the two wire line consist of a twisted or untwisted pair of copper wires. The two bus lines are designated CAN H and CAN L. The digital data are transmitted on both bus lines and represented by a voltage difference [B3]. Bits are transmitted symmetrically when the activated drivers pull the voltage in one circuit to high, and pull the voltage in the other circuit to low.

On the recessive state of the bus, CAN H and CAN L have a small voltage difference, below 50 mV. and the bit 1 is transmitted; whereas in the dominant state, CAN H is pulled high and CAN L is pulled low, thus the bit 0 is sent. For the dominant state, the voltage difference between CAN H and CAN L must be in the rage from 1.5 V to 3.0 V [B11].

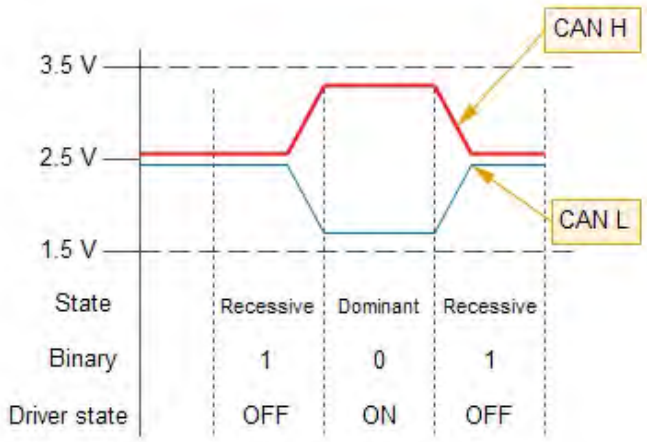

Figure 19: CAN data transmission states.

CAN development
With the same CAN operational principle, different companies offer different evaluation platforms for production software development. In common, software applications and tests are realized through a C based compiler. The environments of development include high level and low level computer languages.

National Instruments development include software as NI LabVIEW, NI LabWindows/C Virtual Instrumentation (CVI) and C/C++. The interfaces for these languages support Universal Serial Bus (USB), Peripheral Component Interconnect (PCI), PCI eXtensions for Instrumentation (PXI) and others [B10].

Texas Instruments also provides development platforms with transceivers and Digital Signal Processor (DSP) of their own. Commonly, the prototyping is realized via USB connection. Compilers for these platforms include Code Composer Studio and C/C++ [B12].

Companies as IXXAT also provide platforms for development and simulation of CAN. USB, Wi-Fi or Ethernet connection is available for IXXAT platforms. The Eclipse compiler, which is also based in C/C++, serve for code debugging in high level [B13].

2.4 MOST standard

MOST Overview

The Media Orientated System Transport (MOST) was developed for networking the infotainment (information and entertainment) in vehicles application. Support a networking up to 64 different devices, MOST posses a point-to-point synchronous data transmission. The MOST cooperation is the organization which creates and manages the specifications for the interfaces and functions of the infotainment applications [B14].

Since 1998, MOST cooperation has developed three generations of data networking. The first generation, MOST25 uses an 1 mm core PMMA fiber. Second generation uses both optical physical layer and electrical physical layer. The electrical physical layer in the second generation is implemented in order to use existing electrical wire components and economize costs. Thus, commonly an unshielded twisted pair of cables is used.

Nowdays, besides the large core POF, the third generation is not completely an optical physical layer, specifications of MOST150 also include coaxial lines. Bit rates and Legacies of the MOST generations are summarized in Table 8.

	Generation	**Physical layer**	**Bitrate**	**Legacy**
1st	MOST25	Optical physical layer (oPhy)	25 Mbit/s	Optical fiber
2nd	MOST50	Optical physical layer (oPhy) Electrical physical layer (ePhy)	50 Mbit/s	POF & Unshielded twisted pair of cables (UTP)
3rd	MOST150	Optical physical layer (oPhy)	150 Mbit/s	POF / LED

Table 8: Summary of MOST generations. Adapted from Ref. [B8].

MOST optical physical layer

MOST network commonly uses a single ring topology Figure 20, and data is transmitted from one device to another. Another MOST topology is the double ring. For the last architecture, two transmitters and two receivers are placed in each node. Therefore, in case of error, redundant segments close the ring, and the MOST network is still functional. At last, some networks posses a combination of star and ring topologies, increasing substantially the performance of the system.

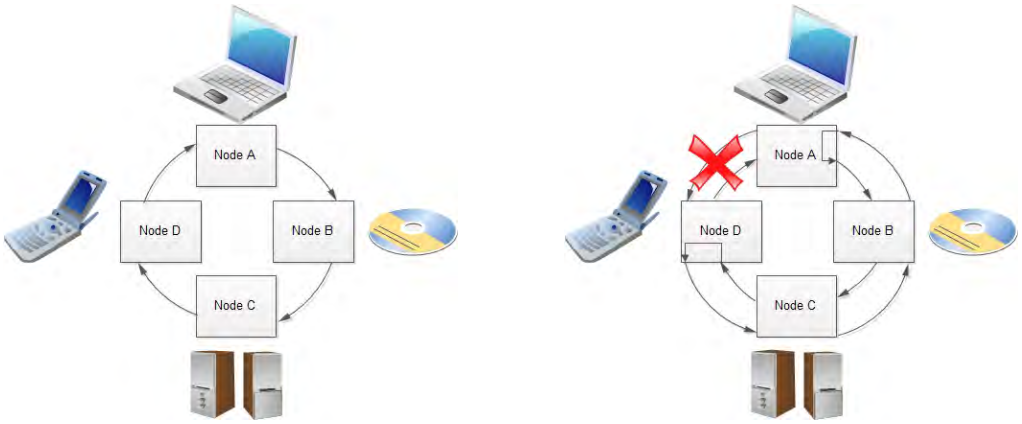

(a) Single ring (b) Double ring

Figure 20: MOST ring topologies. Adapted from Ref. [B8].

Two MOST control modules, defined as MOST Network Interface Controller (NIC), are displayed in Figure 21.

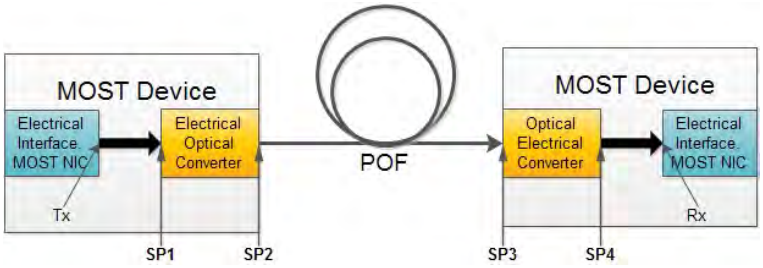

Figure 21: MOST point-to-point connection.

Specifications Points SP1 and SP4 indicate the electrical requirements (as electrical signal levels, connection timeout, electrical ramp response) between

a Network Interface Controller (NIC) and a converter. An electrical/optical converter is used in the SP1 and an optical/electrical converter is used in the SP4. Specifications points SP2 and SP3 describe the interface properties between the MOST device and the transmission medium. In the case of an optical physical layer (oPhy), parameters as wavelength, optical power, plugs mechanical dimensions are defined in points SP2 and SP3 [B8].

In the worst case conditions, while using the optical physical layer, an attenuation of $\alpha = 2$ dB for every connector is still accepted. Nevertheless; the results of employing this large connector attenuation involves that the optical power budget decreases importantly, and the number of devices connected to the MOST network is somewhat limited.

MOST optical communication

The fundamental components of the MOST system includes large core POF as the transmission medium, a LED as the transmitter and a Si photodiode as a receiver. When combining both transmitter and receiver on the same device, obtains the name of Fiber Optic Transceiver (FOT). Figure 22.

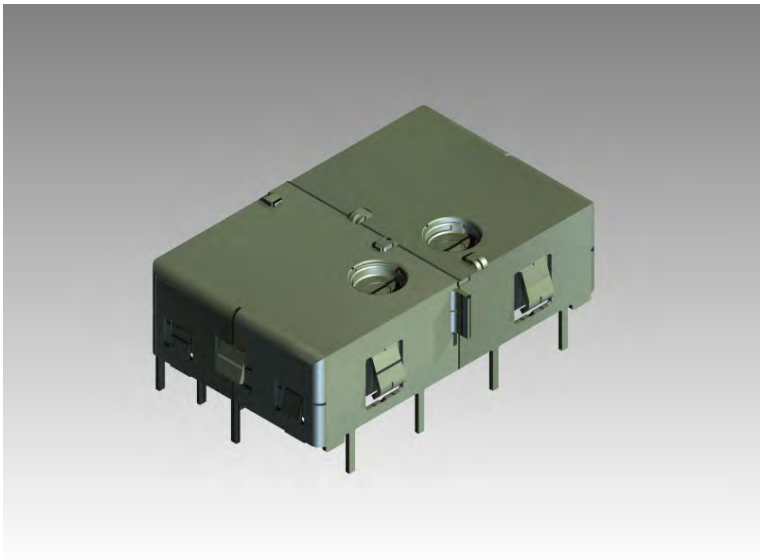

Figure 22: MOST Fiber Optic Transceiver. Ref. [B15].

The LED, as transmitter, converts the electrical signals into optical signals. Commonly, the 650 nm (red) wavelength is used, with the advantage that at this wavelength, the PMMA POF posses a low attenuation peak. Nevertheless, a peak range of $\lambda = 630$ nm to 685 nm, with a 30 nm of Full Width at Half Maximum (FWHM) in the source (transmitter) is accepted in the MOST standard.

The Si photodiode, used as receiver, converts the optical signal into electrical signals. Due to the large core POF, in order to obtain high efficiency in the POF - photodiode coupling, large area photodiodes must be used. Silicon PIN photodiodes type are usually used, which have an operational wavelength range of $\lambda = 400$ nm to 1100 nm, and a typical response of ≈ 0.47 A/W at $\lambda = 650$ nm. An examples of MOST transceiver appear in Figure 23.

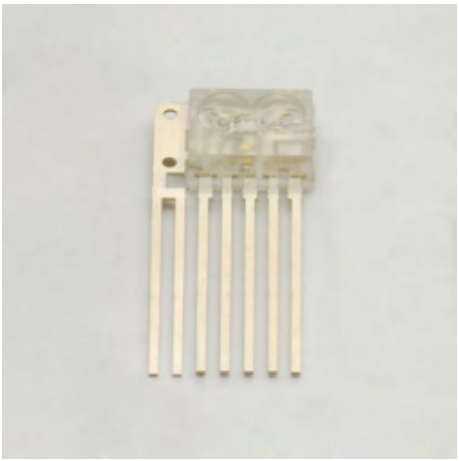

Figure 23: MOST 150 Mbps transceiver by Hamamatsu. Adapted from Ref. [B16].

Commonly, transceivers are packaged into a four pinned plastic case, with a transistor transistor logic (TTL) interface. As in Figure 24, a cavity as interface (CAI) package consist of a LED, a photodiode as receiver and a driver placed altogether in a lead frame. The package is isolated with resin. When plugging the POF to the package, the POF ferrule is aligned into the CAI package, thus obtaining appropriate optical power levels of the system.

MOST 150 supports an Ethernet channel that transport Internet Protocol (IP) data. The legacy Ethernet packets of this channel follows the IEEE 802.3 standard. Besides, through an MOST asynchronous channel, common use network protocols as Transmission Control Protocol/ Internet Protocol (TCP/IP) are enabled. Other protocols as Internetwork Packet Exchange (IPX), NetBIOS Extended User Interface (NetBEUI) and Address Resolution Protocol (ARP) are also enabled [B8].

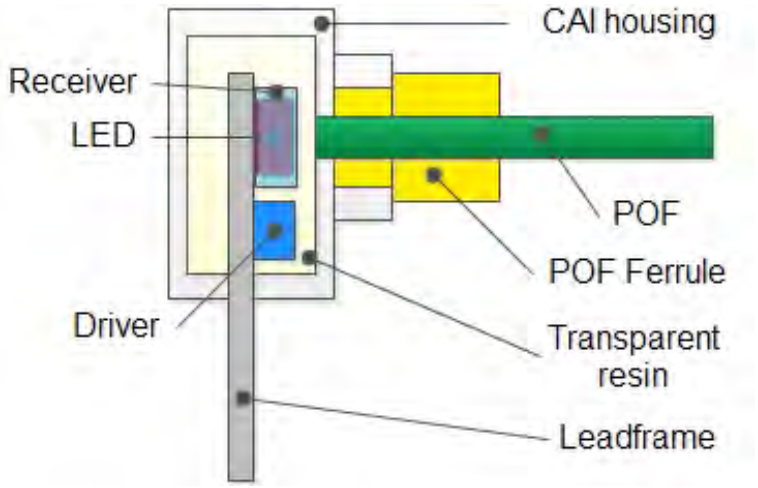

Figure 24: MOST cavity as interface (CAI) package. Adapted from Ref. [B17].

2.5 Other networks

Local Interconnect Network (LIN)

The Local Interconnect Network (LIN) bus was developed as an alternative of the CAN. Firstly introduced in 2001 by Mercedes Benz, the LIN bus serves as a serial bus for the communication of sensors and actuators. Due to electromagnetic interference, the LIN bus is limited to 20 kBit/s, thus a maximum of 16 bus subscribers are allowed.

The LIN communication posses a linear bus topology, where the connections are realized by a single electrical wire. The LIN bus posses a master - slave data transmission, where the master is usually an ECU, and the actuators, sensors and switches are the slaves. Therefore, following a

schedule table, one master node decides which data will be transmitted to the slave nodes bus [B1].

In a LIN network, every electronic control unit is placed in a delimited space. Thus, the LIN serve as a local subsystem which supports the CAN networks [B3]

IDB 1394

The IDB 1394 Network (Intelligent Data Bus 1394) is an automotive network version of the IEEE 1394 standard. When compared with other automotive networks, the IDB 1394 bit rate provides an alternative for the MOST network. This system was developed for networking entertainment and telematic devices, operating a bit rate of 100 Mbps through a twisted pair of copper cables or POF. The topology on the IDB 1394 network is flexible: ring, star, tree or mesh topologies are possible.

Using two plug-in connections, the data is transmitted up to a distance 18 m [B7], whereas the number of nodes subscribed to the bus is limited to 63 [B1].

TTP/C

The time triggered protocol (TTP/C) is a section of the Time Triggered Architecture (TTA). Both TTA architecture and TTP/C protocol were developed by Vienna University of Technology. Automotive applications of the TTP/C protocol are related to the x-by-wire technology, including safety environments like brakes or steering.
In this network, bus and star topologies are available. The data is transmitted by redundant channels; thus every channel carries a copy of the same data. A twisted pair of copper wires serves as the transmission medium.

Byteflight

Introduced by BMW, this bus system was conceived to be used in safety related functions. A common application of the byteflight system is the communication of airbags sensors with other controller units. In this system,

all network nodes are point to point connected to a central active star coupler, developing bidirectional data transmission on the same fiber.

The physical layer developed for this system was based on POF technology [B18], thus, optical and optoelectronic components as fibers and connectors accord with the MOST standard. Parameters as speed, acceleration and pressure of the airbag system are transmitted with a transition rate of 10 Mbps [B7].

Network coupling

In actual vehicles, a single data network can not fulfill all the necessities of computer controlled applications. In addition of the main bus network, other sub-networks realize specific operations. Different networks are not compatible, thus; data can not be transmitted between diverse buses. Therefore, a Gateway is used to read the transmitted data, modify its format and broadcast to other networks. Exchange of data between diverse networks is possible through a Gateway (Figure 25).

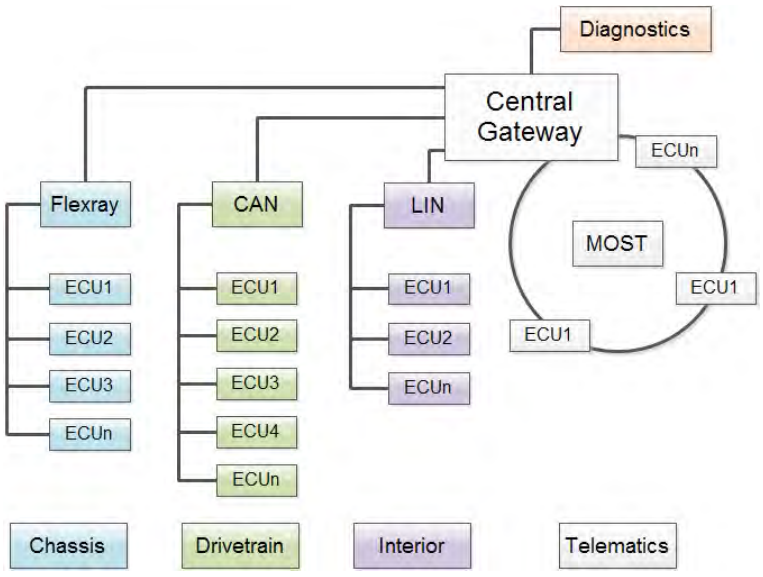

Figure 25: Diverse networks systems are interconnected through a central gateway. Adapted from Ref.[B3].

2.6 Chapter 2 conclusions

- POF provides an optimum cost - benefit relationship for the short optical data links employed in the automotive industry.
- The mainly limitation of the POF in the automotive networks is the temperature. POF are not suitable for applications where temperatures reaches 85 °C or above.
- Automotive networks are not based on only one communication system. According to the application, it is common to find a combination of CAN - MOST and so on, in the same car.

2.7

Chapter 2 References

[B1] Nicolas Navet, Yeqiong Song, Françoise Simonot-Lion, and Cédric Wilwert. Trends in automotive communication systems. *Proceedings of the IEEE*, 93(6):1204–1222, 2005.

[B2] Jurgen Minuth. FlexRay™; electrical physical layer: Theory, components and examples. In *2012 14th International Conference on Transparent Optical Networks (ICTON)*, pages 1–10. IEEE, jul 2012.

[B3] Robert Bosch and Gmbh Ed. *Bosch Automotive Electrics and Automotive Electronics*. Springer Fachmedien Wiesbaden, Wiesbaden, 2014.

[B4] Xuewen He, Qiang Wang, and Zhenli Zhang. A survey of study of FlexRay systems for automotive net. In *Proceedings of 2011 International Conference on Electronic & Mechanical Engineering and Information Technology*, pages 1197–1204. IEEE, aug 2011.

[B5] Eberhard Zeeb. Optical Data Bus Systems in Cars : Current Status and Future Challenges. *Proceedings 27th Erupean Conference on Optical Communications*, pages 70–71, 2001.

[B6] Torsten Schaal, Thomas Kibler, and Eberhard Zeeb. Optical Communication Systems for Automobiles. In *ECOC*, may 2004.

[B7] Olaf Ziemann, Jürgen Krauser, Peter E. Zamzow, and Werner Daum. *POF Handbook Optical Short Range Transmission Systems*. Springer Berlin Heidelberg, Berlin, Heidelberg, 2008.

[B8] Andreas Grzemba. *MOST: The automotive multimedia network; from MOST25 to MOST150*. Franzis Verlag GmbH, 2011.

[B9] Thomas Kibler and Eberhard Zeeb. Optical data links for automotive applications. In *2004 Proceedings. 54th Electronic Components and Technology Conference (IEEE Cat. No.04CH37546)*, pages 1360–1370. IEEE, 2004.

[B10] National Instruments. Controller Area Network (CAN) Overview, 2014. http://www.ni.com/white-paper/2732/en/.

[B11] Barry Hollembeak. *Automotive Electricity and Electronics*. Delmar Cengage Learning, 5th edition, 2011.

[B12] Texas Instruments. CAN Bus Transceivers — Overview — Interface — TI.com, 2016. http://www.ti.com/lsds/ti/interface/can-overview.page.

[B13] HMS Industrial Networks. Overview - Data communication solutions for automotive test systems, 2016. https://www.ixxat.com/products/automotive-products/automotive-overview.

[B14] MOST Cooperation. MOST Cooperation official web site, 2016. http://www.mostcooperation.com/.

[B15] TE Connectivity Ltd. POF,FO PIGTAIL,MOST,FOT UNIT,ASSY: 1-2208264-3 : Fiber Optic — TE Connectivity, 2016. http://www.te.com/usa-en/product-1-2208264-3.html.

[B16] Hamamatsu Photonics K.K. Transmitter photo IC for optical link L11354-01 — Hamamatsu Photonics, 2017. http://www.hamamatsu.com.

[B17] Thomas Kibler, Stefan Poferl, Gotthard Böck, Hans Peter Huber, and Eberhard Zeeb. Optical data buses for automotive applications. *Journal of Lightwave Technology*, 22(9):2184–2199, 2004.

[B18] Josef Berwanger, Martin Peller, and Robert Griessbach. A New Protocol for Safety Critical Applications. *FISITA World Automotive Congress*, (2), 2000.

3 Characterization, cleaving and end termination techniques for POF

The planning of the conducted experiments are shown in this chapter, with focus on increasing temperature termination processes. The low temperature termination methods, where temperatures below -50 °C are needed, change the POF core behavior to practically inelastic. In order to obtain these temperatures, nitrogen and other elements are required [C1]. Low temperature termination methods were not conducted.

3.1 Tools and equipment for POF cleaving

Due to the characteristics of POF, as large core diameter and high dimension tolerances; the manufacture with precision devices could not be so required. Nevertheless, for low losses and standardization, professional tools are always recommended.

Tools for cleaving and stripping POF include razor blades, clippers, scissors, etc. More specialized tools, which can strip and cut plastic optical fiber in the same device, are commercially available.[C2]. In every termination method, dust and undesired particles dramatically increase the insertion loss.

Cleaving fundamentals

While cleaving, the cleaving processes in glass fibers produces three principal regions on a cleaved end face called as *mirror, mist* and *hackle* [C3]. As indicated in Figure 26, The cleave process begins with a small fracture, which propagates to the center of the fiber. The direction of the cleave is the same of the propagation of the fracture.

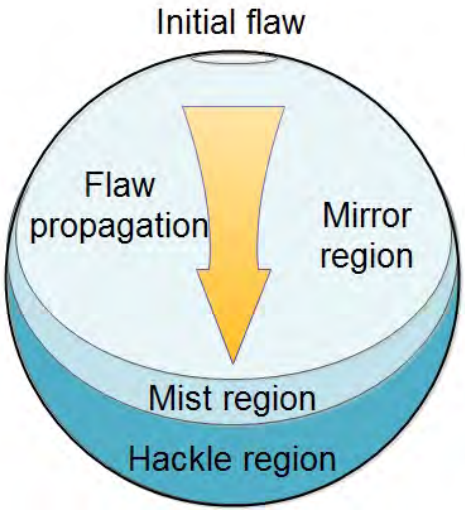

Figure 26: Flaw propagation producing diverse regions on the fiber.

After the fracture, the *mirror region* is formed. This region posses the cleanest and smoothest surface, and therefore, the lowest attenuation. Afterwards, the crack propagation produces the *mist region*, which is a transition zone between the mirror and the hackle zone. By the end, the *hackle region* is undesirable on every cleave. This zone is produced due to the lack of material, thus, the fiber is not properly cleaved, forming a rough surface where chirps and silvers appears.
A good cleave posses low attenuation. Thus, it is desirable that the mirror zone covers as much area of the end face as possible.

Manual tools
Manual tools are referred to non automated cleaving hand tools available. For the cleaving, it was used an ambient temperature of 25 °C.

Razor blade cleaving.
The razor blade cleaving is the most common termination process for POF (Figure 27). Usually, the POF is cut in an orthogonal angle with respect to the blade. In order to maintain this angle, a guide for the POF and blade is used. In ambient temperature, terminations include losses of around 0.68 dB per end face [C4].

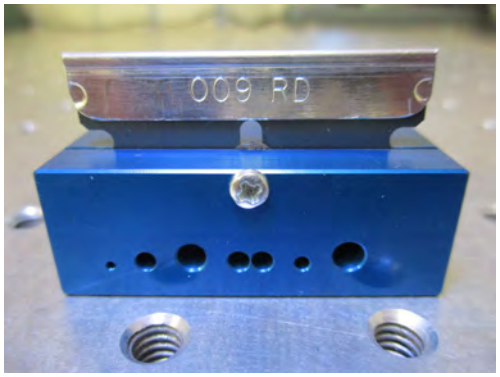

(a) Block shaped razor blade cleaver.

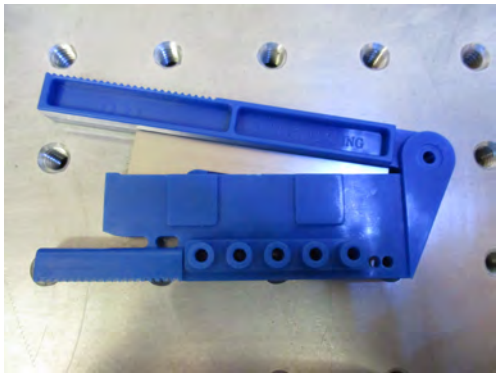

(b) Gullotine functioned razor blade cleaver.

Figure 27: Razor blade cleavers for POF [C5].

In general, the life span of a disposable razor blade is limited to one or two cleaves. It is not suggested reusing the blade more than two times, due to small deformations which appears and increase every time the blade is used. In every cut, the blade is deteriorated and loses its sharpness. For short life span blades, it is suggested to use a virgin section of the blade in every cut [C6].

Blades with a longer life span, can perform several numbers of cuts, this number varies depending the manufacturer. For long life blades; it is recommended to change the section of the blade in every use.

Specialized tools for POF

Hand tools designed for large core POF are commercially available [C2]. On these tools, a circular blade is equipped, and also includes a stripping mechanism which strips the outer jacket, exposing the inner jacket and the core - cladding of the fiber. In comparison with the razor blade, the circular blade also cuts the fiber in a perpendicular position. The manufacturer sets that for every 1260 cuts, a change of blade must be done (Figure 28).

Figure 28: Specialized stripping and cutting tool for MOST POF.

An automated option for stripping and cutting a medium volume of cables is the Omnistrip series (Figure 29). Originally idealized for electrical wires and cables, the Omnistrip machines are capable of strip and cut POF. An adapted version of the Omnistrip machine can automatically process the jackets and the core at specified lengths [C7].

Figure 29: Omnistrip 9450. From Ref. [C7].

It is advisable to use these tools when the cleaving becomes more repetitive. Due to the focused design, it is more expensive to acquire.

Semi automatic cleaving device
A semi automatic cleaving device, locally manufactured, was used to perform cuts with both ambient temperature and controlled temperature. Also, this device is capable of cleave POFs at a controlled speed.

The operation of the semi automatic cleaving device is described as follows. The fiber is stripped, exposing the inner jacket. Then, the fiber is maintained in position with a fiber guide. A mounted circular blade moves in an horizontal direction with a specified constant speed of 1 mm/s. The circular blade cuts the fiber in an orthogonal way (Figure 30).

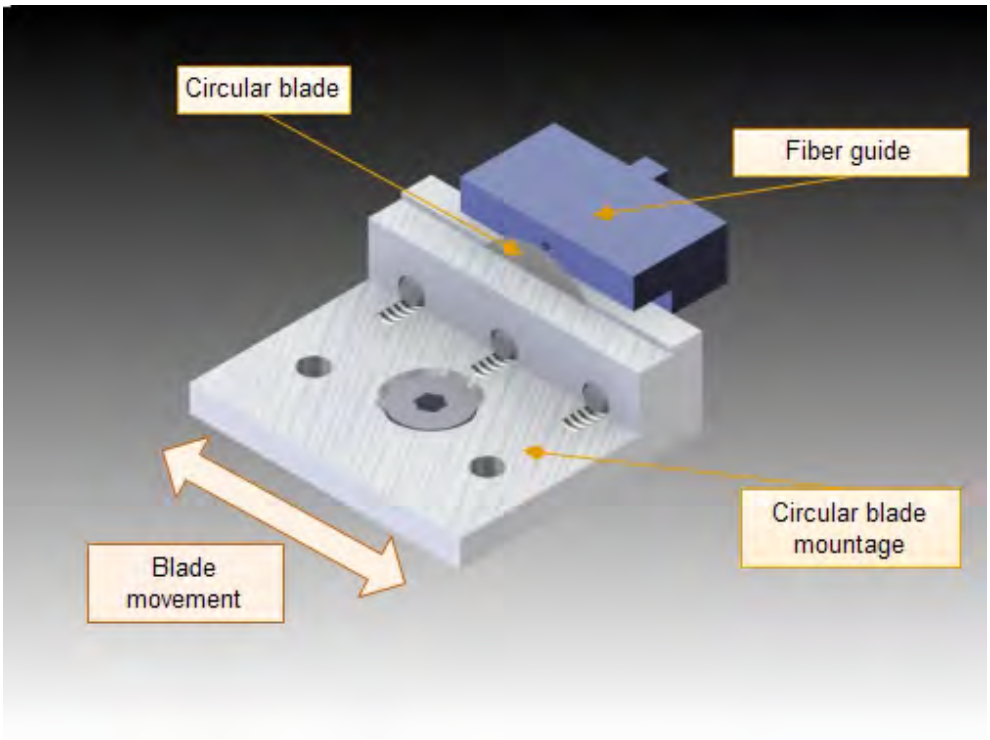

Figure 30: Operation of the semi automatic cleaving device.

It exist a small gap, between the blade and the fiber guide. While increasing the size of this gap, the momentum originated from the fiber and the circular blade is growth. Otherwise, reducing the size of this gap to the minimum helps to reduce the momentum. For a clean cut, a minimum

momentum is desired. As in Figure 31, the actual measure of the gap from the edge of the fiber guide to the cutting edge of the circular blade is 84 μm.

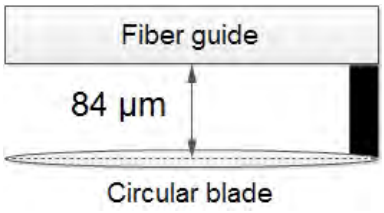

Figure 31: Minimum gap between fiber guide and circular blade.

Temperature on the blade

A common cleaving method is the hot blade, or hot knife cleave. This method includes parameters as the speed of cutting and the temperature of the blade. Using a designed device, the blade is heated until reaching a transition temperature, which change the state of the PMMA fiber core.

On ambient temperature, while cleaving a Si core fiber, due to the brittle properties of the silica, a fracture is propagated through the core. In comparison, using a POF, the PMMA core fiber behaves also in a brittle way. In order to change this behavior of the POF, the blade is heated, provoking that the fiber can be cut as a ductile material [C8].

Based on the MOST standard, the operational limit temperature for the PMMA POF is 85 °C [C9]. Beyond this temperature, the molecular structure of the PMMA is reconfigured.

On isotropic materials, the glass transition temperature (Tg) is in, simplified terms, where its a transition between brittle and ductile behavior appears. Due to small changes of distances between molecules (mainly because its chemical composition and amorphicity grade), there is no exact Tg. For PMMA, several authors have set Tg between 105 °C and 128 °C using as a not declared standard 120 °C [C10], [C8], [C11], [C12] and even one author reported 80 °C [C13]. However, the melting temperature process of PMMA is found at 128 °C [C14], although for its thermoforming processing is typical to use from 200 °C to 200 °C.

For this method, it was assembled a closed loop temperature controller, (Figure 32) which monitors the blade temperature and energize the heating resistance. The blade temperatures used were 25 °C, 90 °C and 120 °C.

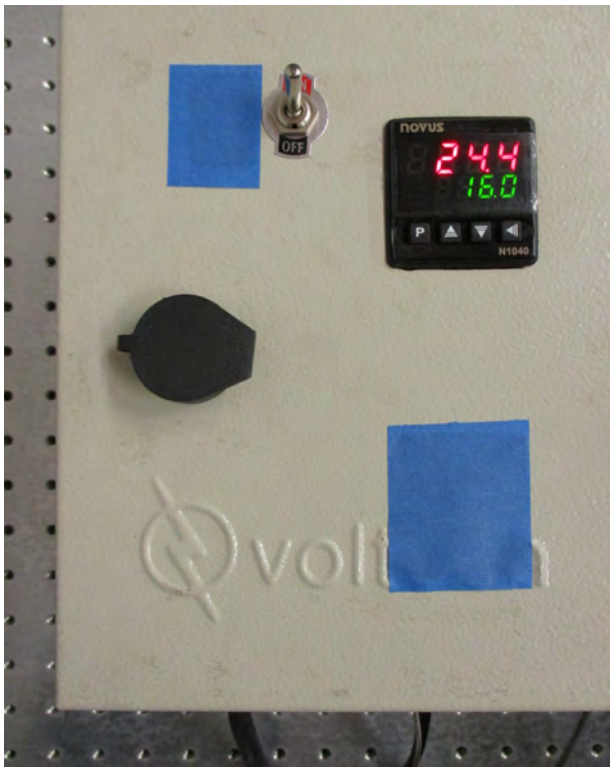

Figure 32: Closed loop temperature controller.

The hot blade cleaving system includes a type K thermocouple and a cartridge type electric heating resistance, which are both controlled by a temperature controller. The circular blade moves in a horizontal axis, and cuts the fiber with a right angle with respect to the transversal axis of the fiber. Thermal paste was used to improve the contact of the heated elements (Figure 33). Once again, the distance from the edge of the fiber guide, to the cutting edge of the circular blade is 84 μm.

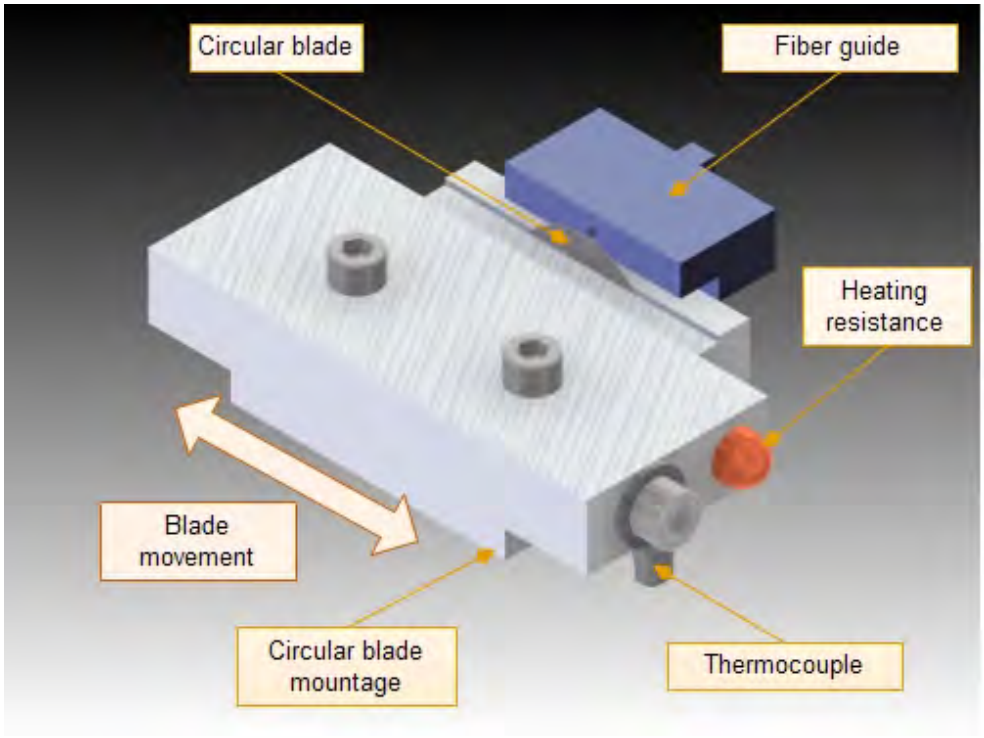

Figure 33: Hot blade cleave operation.

Temperature on the fiber.
In order to obtain a clean cross section of the fiber, the temperature of the fiber is increased, expecting a ductile behavior of the core material. Another advantage of increasing the fiber temperature is the reduction of the blade damage.

When using hot air, the fiber was heated by convection (Figure 34). The circular blade moves on the horizontal axis, and cleaves the heated fiber with a perpendicular angle. The distance between the edge of the fiber guide and the cutting edge of the circular blade is maintained in 84 μm.

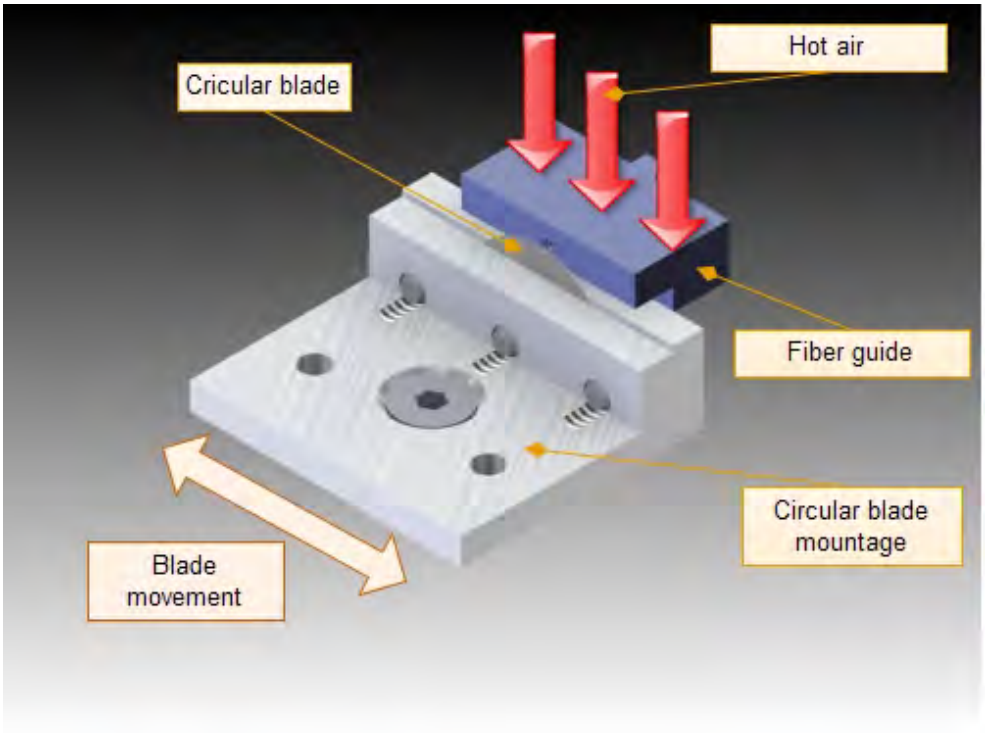

Figure 34: Temperature increase of the POF.

3.2 POF end face termination

Hot plate termination
In general terms, the hot plate termination method consist in melting the end face of the fiber, which was previously cut. The end face is pressed against a heated plate, and flattened.

The heated plate must be a mirror surface, with a temperature beyond the transition state. On a 125 μm POF, the temperature is $\approx$ 120 °C [C12]. Commercially available devices designed for this method, use a temperature range of 150 °C to 200 °C [C15].

After the fiber has been stripped, the ferrule is inserted and the fiber is fixed here and/or at the end of the termination by hot plate. A small protrusion of the exposed core is required. This protrusion must have a grater length than the ferrule. Afterwards, the fiber is cut and a resin is

applied if necessary. The small protrusion is needed in order to fill the voids of the ferrule when melted.

The fiber is pressed for a short period of time, typically less than 10 seconds. In this operation, the surface of the hot blade shapes the end face of the POF. In order to avoid particles and dust that could get printed onto the fiber's core, the mirror surface must be completely clean (Figure 35).

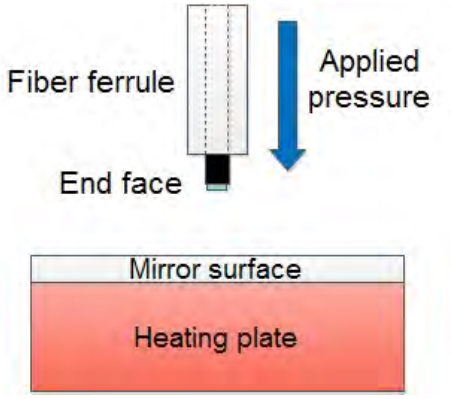

Figure 35: Hot plate termination schematic.

Polishing POF

The polishing procedure includes aggressive polishing films that remove both core and clad material. With this method, the end face of the POF is flattened and imperfections are removed.

Required parts and tools

The next list includes tools used in the polishing procedure.

- Lint free wipes.
- Canned air.
- Distilled water.
- Glass polishing plate.
- Rubber polishing pad.

- Polishing disc.
- Polishing films.

The polishing films used include the sizes: 12 μm (yellow), 5 μm (brown), 3 μm (pink), 1 μm (green) and 0.5 μm (white).

Polishing procedure

1. The rubber polishing plate, and the bottom face of the polishing disk are cleaned by using distilled water (or isopropyl alcohol) and lint free wipes.
2. A previously cleaved fiber is inserted into the polishing disc. A small overlenght of the POF cable exits the bottom of the polishing disc.
3. The polishing film is placed with the bright side towards the polishing plate, avoiding air bubbles or other irregularities. The polishing procedure begins with a rough grain size, in this case with a 12 μm (yellow color) polishing film.
4. The movements of the polishing disc follows an 8 figure pattern. It is recommended to cover the whole area of the polishing film.
5. The polishing film is changed to a smaller grain size. Every change of polishing film, the fiber's polished end face and the polishing disc must be cleaned with canned air. The polished end face is inspected.
6. After using the last polishing film, the polishing disc and the rubber pad must be cleaned with distilled water (or isopropyl alcohol) and lint free wipes.[C16]

3.3 Optical power loss measurement techniques

In general terms, the POF attenuation is quantified by the optical power loss. It is supposed that the POF attenuation coefficient (α) remains constant through the length of the fiber. The cutback technique is commonly used for measure the overall attenuation on a fiber.

Cutback method

In the cutback method; the transmitted intensity through a fiber is measured. Then, a certain length is removed, and the intensity is measured once again.

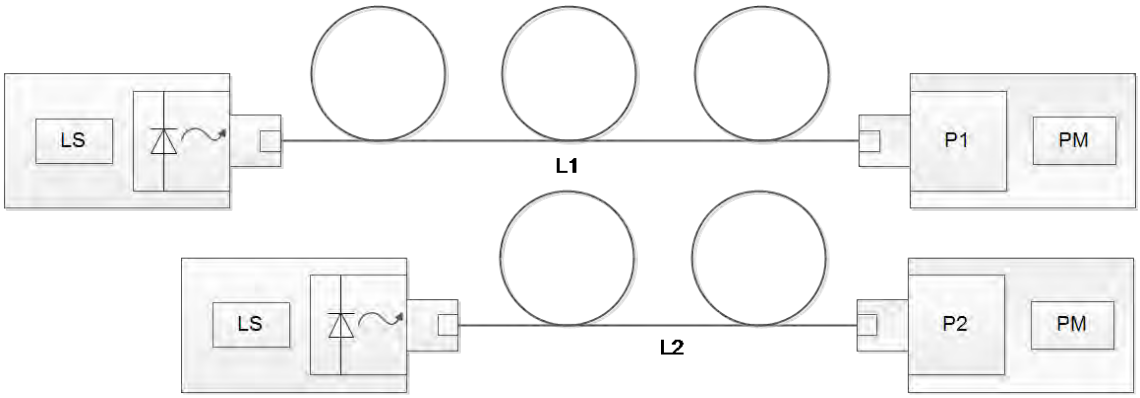

Figure 36: Cutback measurement schematic.

Legend			
LS	light source	L1	length 1
L2	length 2	PM	power meter

Figure 36 shows the cutback technique [C17]. With a smaller length of fiber removed, which increments the number of measurements, more certainty in the result is achieved. The objective of this test is to obtain the insertion loss of the fiber. This is expressed by:

$$\alpha = \frac{\ln\left(\frac{P_2}{P_1}\right)}{L_1 - L_2} \tag{17}$$

Where P_1 and P_2 represents the first and the second measurements of the optical power coupled into the fiber. L_1 and L_2 serve as the first and the second length of the fiber. [C18]

Multimode fiber attenuation measurement

According to the TIA-526-14-B [C19], the two cord reference method, formerly known as Method A in OFSTP-14-A, was employed in order to obtain the cable losses.

A light source, power meter and test cords are required in this method.In the two cord reference method, includes the loss of one of the connections of the cable under test. The procedure is described as followed:

- The launch cord (TC1) and receive cord (TC2) are connected to the light source and power meter respectively.
- The launch cord (TC1) and receive cord (TC2) are connected to each other.
- The measured optical power (P1) is measured. P1 is used as the reference power measurement (Figure 37).
- Without disconnecting TC1 from the light source, the cable under test is inserted.
- The optical power P2 is measured, and recorded (Figure 38).

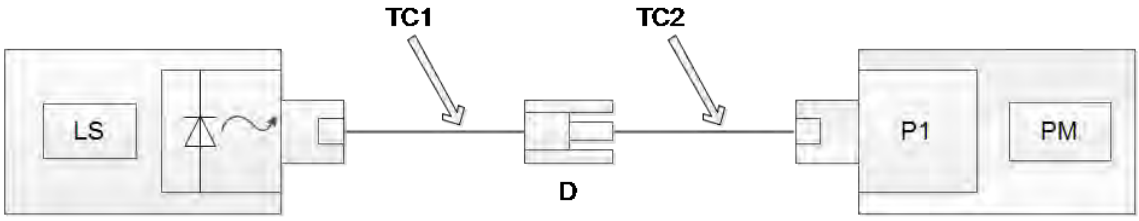

Figure 37: Reference measurement schematic.

Legend			
LS	light source	TC2	receive cord
TC1	launch cord	PM	power meter
D	inline connector		

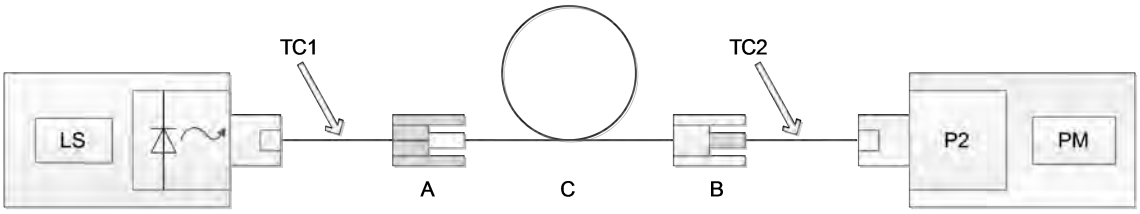

Figure 38: Test measurement.

Legend			
LS	light source	TC2	receive cord
TC1	launch cord	PM	power meter
C	cable under test	A, B	inline connector

Even with the manufacturers specifications, in this dissertation it was discovered that, for the operational wavelength of the light source, was displaced several nanometers, with a peak wavelength at 637 nm. The silicon detector is completely functional at this wavelength.

In every essay realized in this work, the length of the fiber was the same, (2.25 m). The following table describes the equipment used in the optical cable power loss test.

Equipment	**Summary**
Light source	Operational wavelength 650 nm (nominal). Optimized for POF
Power meter	3 mm Silicon detector type. Optimized for POF
Inline connector	A guided protective case and a catch mechanism used to connect the cables. Optimized for POF
Launch cord and receive cord	Cords used to reference the measurements in the test. It is advisable that the length of each cord shall not exceed the length of the cable under test. The launch and receive cord must be of the same type of the cable under test

Table 9: Equipment used in POF loss test.

To avoid losses due to bending in the MOST PMMA core fiber, it is

recommended that the minimum bending radius equals to 25 mm. A smaller radius will increase the losses, besides provoking physical damage to the fiber (Figure 39) [C9].

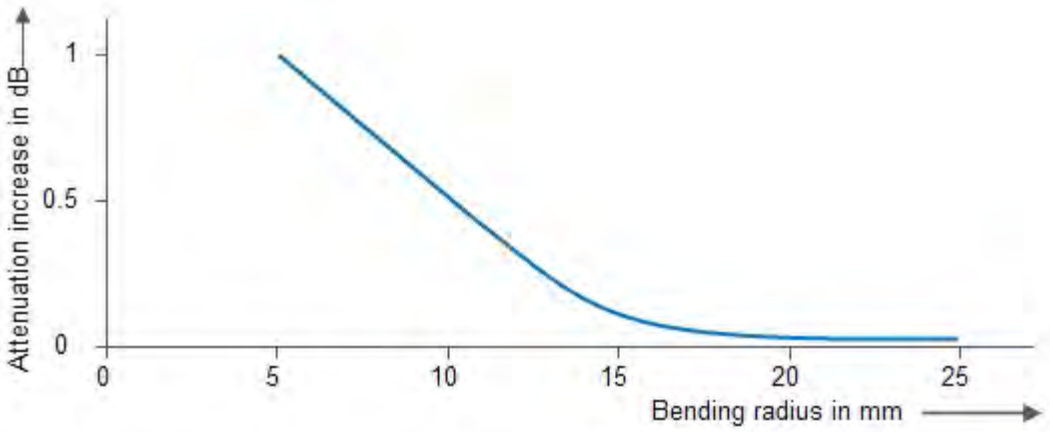

Figure 39: Bending losses in POF. Adapted from Ref. [C20].

A circular base was manufactured for the purpose of obtaining repeatability of the measurements. This base was designed in order to loop the fiber on the center with a constant diameter. The circular base and the legs are made of plastic. (Figure 40).

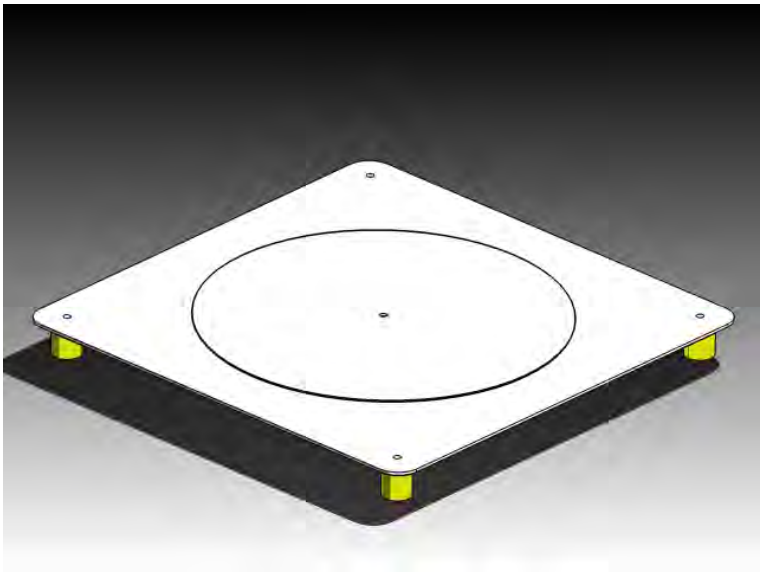

Figure 40: Plastic circular base.

Connection of POF

Diverse methods of POF - ferrule contact are available; The fixation method varies depending on the mechanical stability required for the fiber. The next table displays some of the contact technologies used in PMMA core POF. In every method mentioned, the fixation is permanent.

Ferrule material	**Method of connection**
Brass	Crimp
Plastic	Ultrasonic welding
Plastic (transparent)	Laser welding

Table 10: Contact methods for POF-ferrule.

On the crimping method, a metallic ferrule, generally made of brass, is used. For the ultrasonic welding, the plastic ferrule inner diameter is melted on the POF buffer. On the other hand, a different kind of ferrule, transparent for the operational wavelength of the laser, is needed in the laser welding [C9].

3.4 Splicing losses

The splicing losses make reference to the quantity of light lost in the connection of two end faces placed each other. There exist several reasons that originate and increase these losses (Figure 41). In an ordinary connection, one or more of these factors can appear.

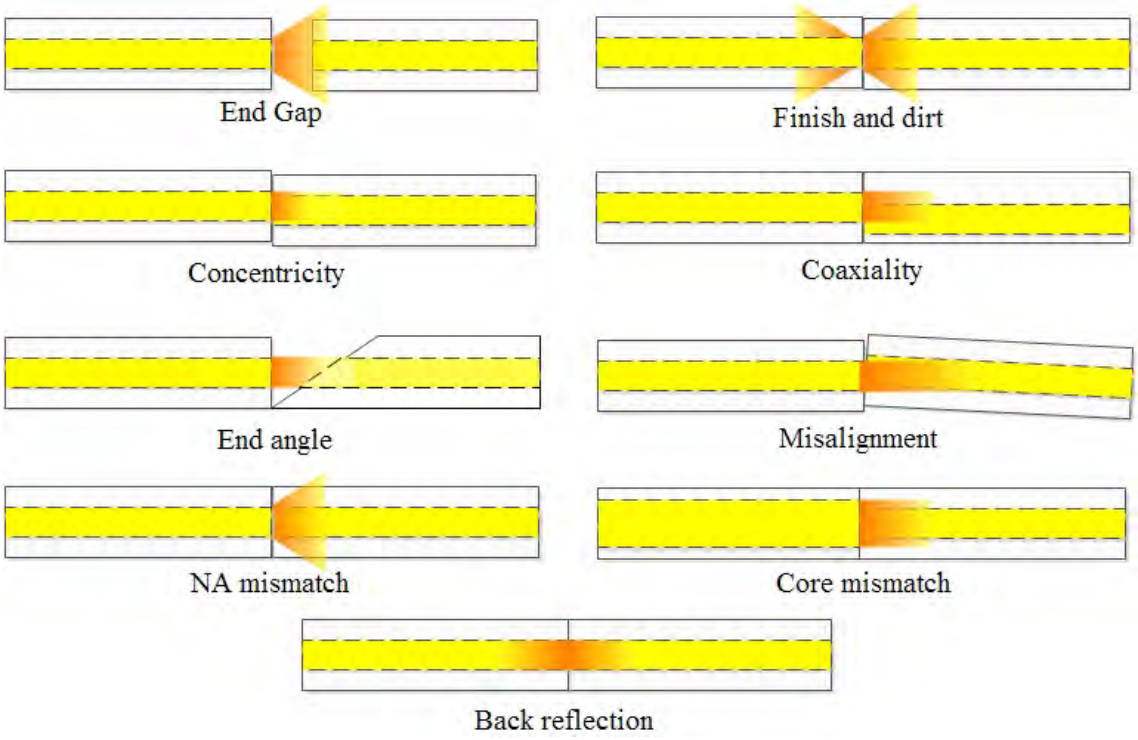

Figure 41: Connector losses.

The major causes of the connection losses includes:

- Misalignment of the ends of the fiber, in one or more directions.
- Differences in the fiber's parameters.
- Fresnel reflection.

Misalignment of the ends of the fiber

There exist three types of misalignment at the end of the fiber: *Axial displacement, longitudinal separation* and *angular misalignment.*

Axial displacement.
Also known as lateral displacement, occurs when the two axes of the fiber are separated by a distance d. Figure 42

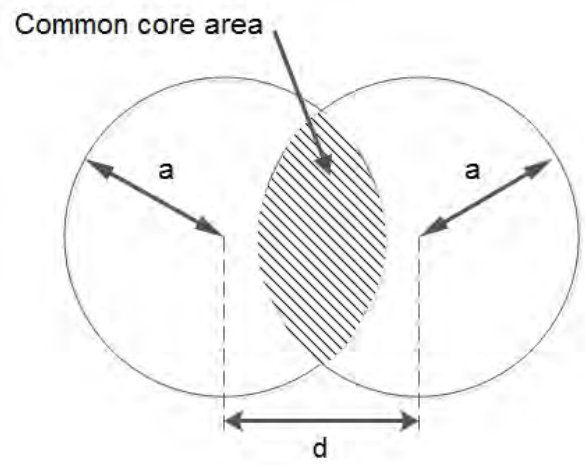

Figure 42: Axial displacement of two fibers.

Supposing two identical step index fibers with radii a, and a separation d; the optical power coupled from one fiber to another is relative to the common area A_{comm}, as:

$$A_{comm} = 2a^2 \arccos \frac{d}{2a} - d\left(a^2 - \frac{d^2}{4}\right)^{\frac{1}{2}} \tag{18}$$

Longitudinal separation.
The longitudinal separation refers as the non axial distance between the two fiber ends, separated by a gap s. Figure 43

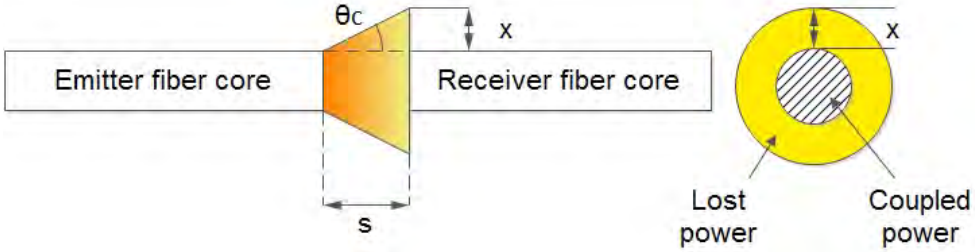

Figure 43: Longitudinal separation of two fibers.

For a step index fiber, the loss due to longitudinal separation is expressed as in:

$$L_F = -10 \log \left(\frac{a}{a + s \tan \theta_c} \right)^2 \tag{19}$$

With θ_c as the critical angle, known as:

$$\theta_c = \arcsin \left(\frac{n_2}{n_1} \right) \tag{20}$$

Angular misalignment
Losses arises from the angular misalignment when the optical power from the emitting fiber propagates beyond the solid acceptance angle of the receiving fiber. With an angle of misalignment θ of two step index fibers, the angular misalignment loss can be declared as:

$$L_F = -10 \log \left(\cos \theta \left\{ \frac{1}{2} - \frac{1}{\pi} p(1-p^2)^{\frac{1}{2}} - \frac{1}{\pi} \arcsin p - q \left[\frac{1}{\pi} y(1-y^2)^{\frac{1}{2}} + \frac{1}{\pi} \arcsin y + \frac{1}{2} \right] \right\} \right) \tag{21}$$

where

$$p = \frac{\cos \theta_c (1 - \cos \theta)}{\sin \theta_c \sin \theta} \tag{22}$$

$$q = \frac{\cos^3 \theta_c}{\left(\cos^2 \theta_c - \sin^2 \theta \right)^{\frac{3}{2}}} \tag{23}$$

$$y = \frac{\cos^2 \theta_c (1 - \cos \theta) - \sin^2 \theta}{\sin \theta_c \cos \theta_c \sin \theta} \tag{24}$$

Differences in the fiber's parameters
Differences in parameters such as core diameter,numerical aperture, or coaxiality (ellipticity of the core) in any of the two joined fibers produces significant losses. Larger losses are produced by differences in core radii and numerical aperture mismatch than the coaxiality of the joined fibers [C4].

Fresnel reflection

Also known as back reflection, the Fresnel reflection is caused by the change of refractive index in the interface POF core - air. This reflection produces a return loss in the optical waveguide. The reflection coefficient is expressed as:

$$R = \left(\frac{n_{core} - n_{air}}{n_{core} + n_{air}} \right)^2 \tag{25}$$

Where n_{core} and n_{air} represents the refractive index of the core and the air. With values of $n_{core} = 1.492$ for a PMMA POF and $n_{air} = 1.0$, the reflection coefficient is ≈ 0.04. With these values an estimation for the transmission coefficient is:

$$T = 1 - R \approx 0.96 \approx 0.17 \text{ dB} \tag{26}$$

Thus, a single end face Fresnel reflection will cause an optical power loss of 0.17 dB in a PMMA POF [C20].

3.5 Chapter 3 Conclusions

- In glass optical fibers, is mandatory the usage of precision devices which implies high costs. In comparison, the geometric tolerances of POF diminish the costs of tools and equipment.

- Razor blade cleaving is the most common cleaving process for POF. In this process, the life span of a blade is limited to two cuts as maximum.

- In order to obtain a clean cross section of the POF, diverse termination methods are used. Methods which involves increments of temperature are conducted in the interest of changing the PMMA core material behavior from brittle to ductile.

- Decreasing the POF temperature below -50 °C will produce a fundamentally inelastic POF core behavior. In order to achieve these temperatures, nitrogen and other elements are needed.

- Splicing losses can be easily diminished with an appropriate alignment of the end face axes.

3.6

Chapter 3 References

[C1] Marcelo Vaca Pereira Ghirghi, Vladimir P. Minkovich, and Armando Garcia Villegas. Polymer optical fiber termination with use of liquid nitrogen. *IEEE Photonics Technology Letters*, 26(5):516–519, 2014.

[C2] Rennsteig. Rennsteig Tools, Inc. - Tool for stripping and cutting polymeric optical fibers system MOST, 2016. `http://www.rennsteig.us`.

[C3] D. Andrew Yablon. *Optical Fiber Fusion Splicing*, volume 103 of *Springer Series in Optical Sciences*. Springer-Verlag, Berlin/Heidelberg, 2005.

[C4] Olaf Ziemann, Jürgen Krauser, Peter E. Zamzow, and Werner Daum. *POF Handbook Optical Short Range Transmission Systems*. Springer Berlin Heidelberg, Berlin, Heidelberg, 2008.

[C5] FiberFin. Low Cost POF Finishing, 2017. `http://www.fiberfin.com`.

[C6] M. A. Losada, F. A. Domínguez-Chapman, J. Mateo, A. López, and J. Zubia. Influence of termination on connector loss for plastic optical fibres. *International Conference on Transparent Optical Networks*, 1000:5–8, 2014.

[C7] Schleuniger. Schleuniger in North America, 2017. `http://www.schleuniger-na.com/en-us/`.

[C8] S H Law, M A van Eijkelenborg, G W Barton, C Yan, R Lwin, and J Gan. Cleaved end-face quality of microstructured polymer optical fibres. *Optics Communications*, 265(2):513–520, sep 2006.

[C9] Andreas Grzemba. *MOST: The automotive multimedia network; from MOST25 to MOST150.* Franzis Verlag GmbH, 2011.

[C10] Danielle Mathiesen, Dana Vogtmann, and Rebecca B. Dupaix. Characterization and constitutive modeling of stress-relaxation

behavior of Poly(methyl methacrylate) (PMMA) across the glass transition temperature. *Mechanics of Materials*, 71:74–84, 2014.

[C11] O. Abdi, K. C. Wong, T. Hassan, K. J. Peters, and M. J. Kowalsky. Cleaving of solid single mode polymer optical fiber for strain sensor applications. *Optics Communications*, 282(5):856–861, 2009.

[C12] Van Hove, T Coosemans, B Dhoede, P Van Daele, R Baets, J Van Koetsem, and Framatome Connectors International. Termination olf Small Diameter (125 um) Plastic Optical Fiber for 1x12 Datacommunication. pages 783–789, 1998.

[C13] A Stefani, K Nielsen, H K Rasmussen, and O Bang. Cleaving of TOPAS and PMMA microstructured polymer optical fi bers : Core-shift and statistical quality optimization. *OPTICS*, 285(7):1825–1833, 2012.

[C14] J. L. Pérez-Castellanos, D. S. Montero, C. Vázquez, J. Zahr-Viñuela, and M. González. Photo-Thermo-Mechanical Behaviour Under Quasi-Static Tensile Conditions of a PMMA-Core Optical Fibre. *Strain*, 52(1):3–13, 2016.

[C15] FiberFin. Hot Plate Termination, 2016. `http://www.fiberfin.com`.

[C16] Thorlabs. FN96A Guide to Connectorization and Polishing Optical Fibers • Cable Assembly • Manual Fiber Polishing • Manual Fiber Cleaving. Technical Report December, Thorlabs, 2015. `https://www.thorlabs.com/`.

[C17] Dennis Derickson. *Fiber optics test and measurement*. Prentice Hall PTR, Upper Saddle River, 1998.

[C18] Rongqing Hui and Maurice O'Sullivan. *Fiber Optic Measurement Techniques*. Elsevier, 1st edition, 2009.

[C19] Telecommunications industry association. *Optical Power Loss Measurements of Installed Multimode Fiber Cable Plant ; IEC Communications Subsystem Test Procedure- Part 4-1 : Installed cable plant- Multimode attenuation measurement October 2010*. Number October. TIA Telecommunications Industry Association Standard and Engineering Publications, 2010.

[C20] Andreas Weinert. *Plastic Optical Fibers: principles, components, installation*. Publicis MCD Verlag, Berlin, 1999.

4 Experimental Results

4.1 Light source characterization

For the insertion loss measurement, as described in Chapter 3, an OS417-MD LED source was used. According to the manufacturer, the LED source is optimized for large core POF, and the nominal operational wavelength of the source is $\lambda = 650$ nm. Nevertheless, a displacement in the wavelength peak was detected. The following Figure 44 shows this wavelength shift respect to the reference wavelength of 650 nm.

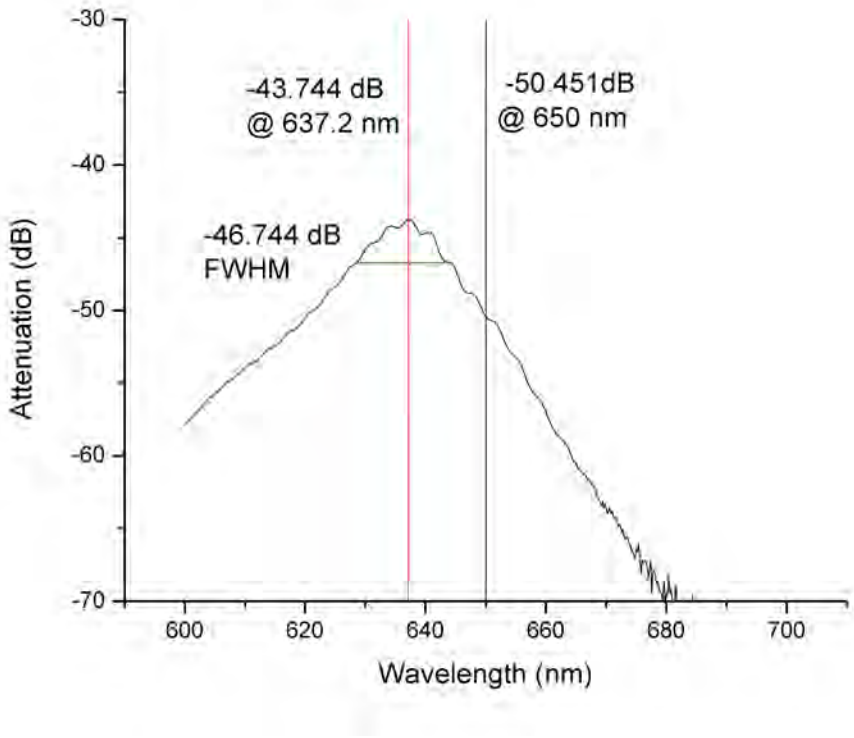

Figure 44: Power spectrum emission of the LED source.

In Figure 44, an optical power difference of 6.707 dB arise between the reference wavelenght and the LED source wavelength. This power spectrum was realized with an AQ6315-A optical spectrum analyzer. The Full Width

at Half Maximum (FWHM) of the power spectrum was set at -46.744 dB, covering a wavelength range of 15.8 nm; from 628.5 nm to 644.3 nm.

The wavelength shift of the central peak generates a different insertion loss behavior. Due to the dependency of the intrinsic attenuation response of the POF to the wavelength, the peak parameter $\lambda = 637$ nm. was taken as the operational wavelength through the plastic optical fiber cable proofs.

The LED source posses an optical power of 1.3 mW. at 635 nm. Numerical aperture of the LED source was measured to 5% of the optical power peak, giving as a result ≈ 0.1. The fiber optic power meter is also optimized for large core POF. The 3 mm squared silicon detector is compatible with the 637 nm operational wavelength.

Geometric parameters

As described in Chapter 1, the typical POF diameters of the core and cladding are 980 μm and 1000 μm, respectively. For the MOST system, the inner jacket, made of Polyamide 12 (PA-12), posses a typical diameter of 1510 μm. According to the manufacturer, the concentricity to the POF cable does not surpass 60 μm. After cleaving, the last parameter is not exceeded.

Figure (45) shows the displacement of the concenctricity of the POF, where the inner jacket is mostly deformed. With the use of Matlab® software and a microscopy camera, images of the POF end face were acquired and digitally processed. Following the Young's Modulus, the PA-12 material is more flexible than the PMMA material. The last difference indicates that the inner jacket strains easier than the core.

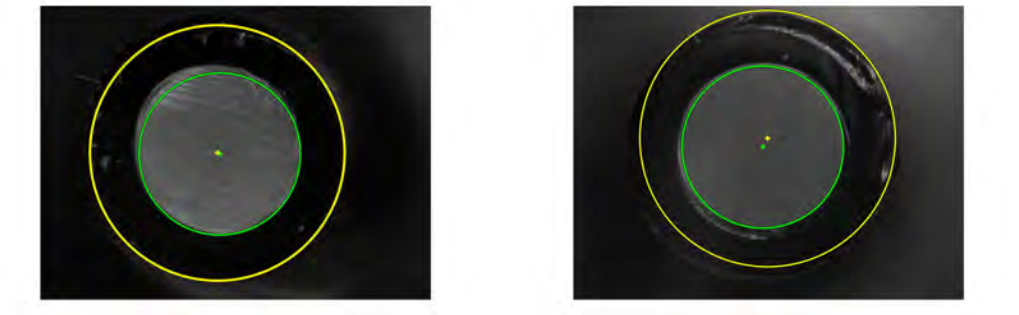

(a) Concentricity displacement of ≈ 15 μm. (b) Concentricity displacement of ≈ 55 μm.

Figure 45: Geometric center displacement for the core - cladding and inner jacket perimeters.

A section of the sharp edge from the circular blade, used in the semi automatic cleaving device, is shown in Figure 46. In POFs, after removing the outer jacket, the fiber cross section is smaller than the radius of the blade. When using ductile materials, the tip edge of the blade performs the cut. Damage to the end face of the POF is caused by the blade itself.

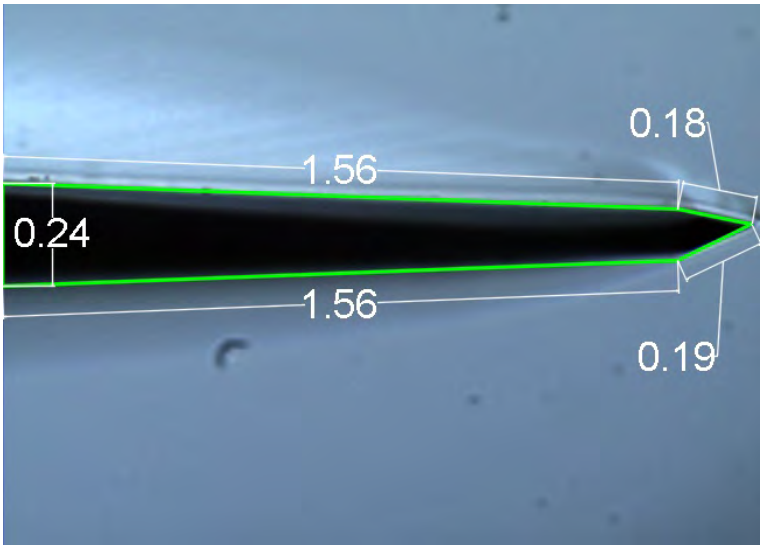

Figure 46: Sharp edge dimensions of the circular blade. Units in mm. Not to scale.

With a thicker sharp edge, the blade is able to perform more cleaves.

Nevertheless, a thicker sharp edge is not able to perform end faces as clean as a thinner edge.

4.2 Spectral attenuation characterization of the POF cable

The POF used along the experiments was MOST PMMA POF, which characteristics were described in the Chapter 1. Fiber from the same manufacturer (Mitsubishi) was acquired in two batches. The following results are presented according to the optical spectrum analyzer resolution.

The fiber characterization involves the cutback method, previously described in Chapter 3 of this work. Because the cable maximum length used in the automotive industry is commonly limited to 20 meters, dispersion test were obviated.

Technical data
Following the Figure 47, the typical loss spectra for the Datacom grade POF. at the operational wavelength $\lambda = 637$ nm. is approximately $\alpha = 0.24$ dB/m. Depending on the manufacturer, this number could slightly change.

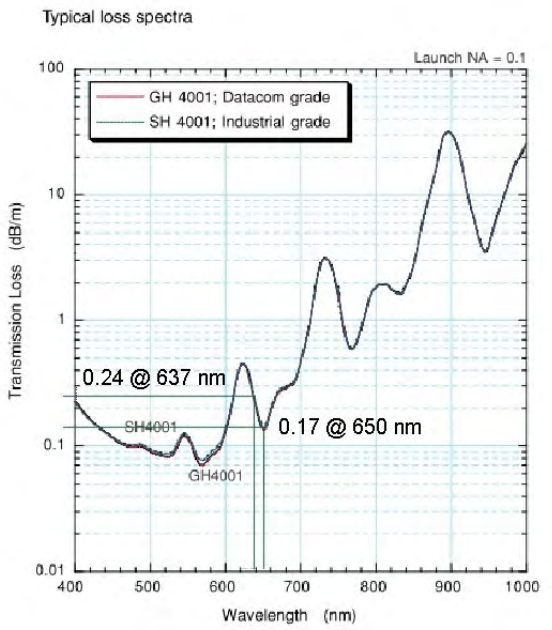

Figure 47: POF attenuation spectra. Ref. [D1].

In this work, two different resolutions, from the optical spectrum analyzer, were used in the cutback method: 5 nm. resolution and 1 nm. resolution. According to the cutback method procedure, described in Chapter 3, fiber from the light source end point was removed (Figure 48). In the realized cutback measurements, the POF length L1 was coiled with a diameter above 30 cm, maintaining restricted L2. The length of L2 was set to 1 meter in a straight fixed position. Figures 49 and 50 were realized with an AQ6315-A optical spectrum analyzer as the power meter (PM), and a white light source AQ-4303B which served as the light source (LS).

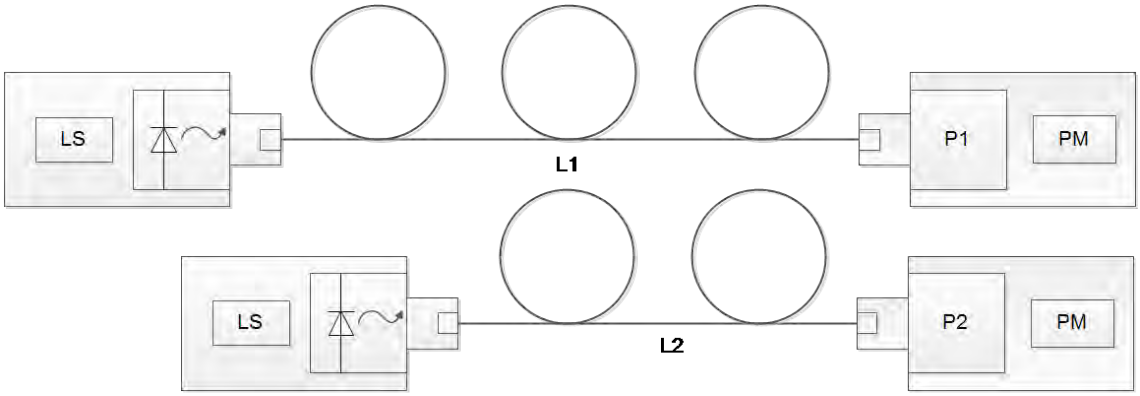

Figure 48: Cutback measurement. Repeated from Chapter 3.

Legend			
LS	light source	L1	length 1
L2	length 2	PM	power meter

5 nm. resolution results

In the Figure 49 appears four different lines, the first three curves, *Aa (50 m), Ab (47 m)* and *Ac (18 m)*, correspond to the cutback method conducted on the fiber at 50 m, 47 m. and 18 m. respectively, with a resolution of 5 nm. The last curve *Ad (Avg)* corresponds to the average of the three previous curves.

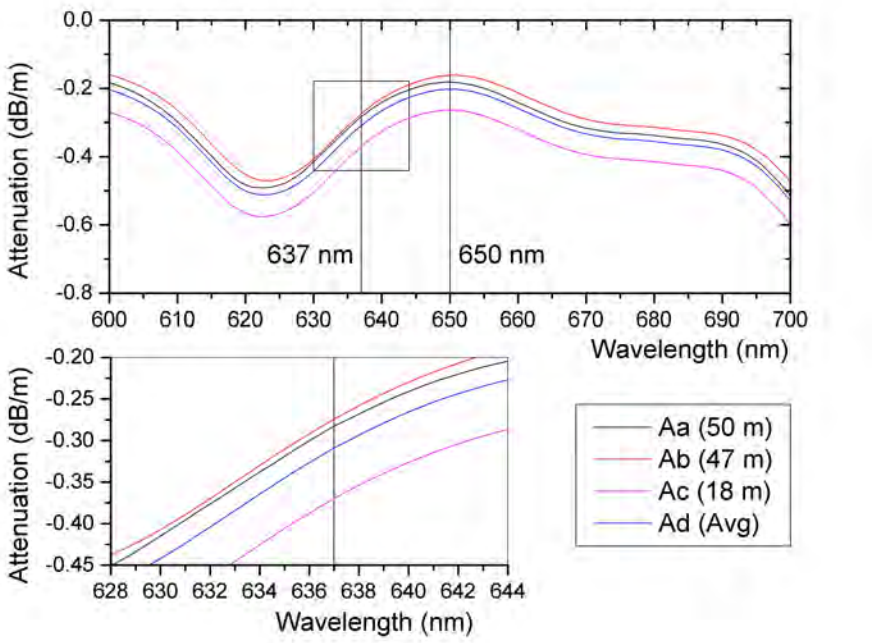

Figure 49: Attenuation spectra plot for 5 nm. resolution.

An important difference in attenuation arises from the wavelength shift of the operational wavelength. Due to the slope, the displacement to a shorter wavelength produces an increment in the attenuation of more than 0.1 dB/m.

1 nm. resolution results

In the Figure 50, the first two curves *Ba (47 m)* and *Bb (18 m)* indicate the the cutback method realized at 47 m. and 18 m. respectively.

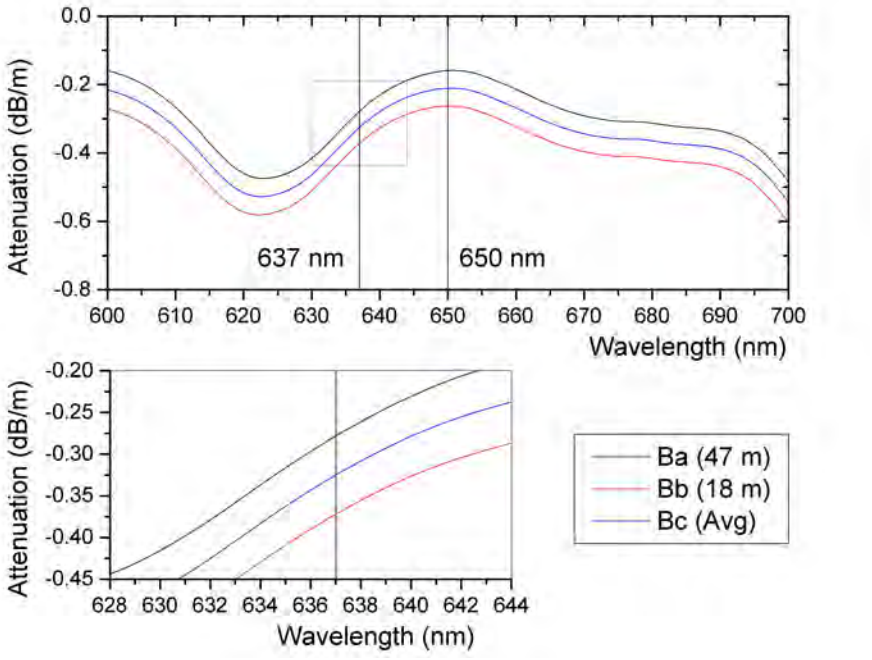

Figure 50: Attenuation spectra plot for 1 nm. resolution.

The average of the previous two curves on Figure 50 is displayed in the curve *Bc (Avg)*. Because of the slope, the displacement of the operational wavelength produces an increase of more than 0.1 dB/m. In comparison with the 5 nm. resolution, the 1 nm. resolution presents a slightly raised attenuation. The next table shows a summary of both resolutions data.

λ (nm)		637	650
	Aa (50 m)	-0.28245	-0.1821
	Ab (47 m)	-0.27428	-0.16157
	Ac (18 m)	-0.36967	-0.26335
	Ad (Avg)	-0.3088	-0.20234
α (dB/m)	Ba (47 m)	-0.27819	-0.15901
	Bb (18 m)	-0.37207	-0.26259
	Bc (Avg)	-0.32513	-0.2108
	Manufacturer Reference	-0.24	-0.17

Table 11: Summary of attenuation at 637 nm and 650 nm from the cutback method.

Due to the attenuation levels, the next conducted tests were performed with 5 nm. resolution data. Attenuation at 637 nm differs from the manufacturer's data in an increase of $\approx 29\%$. Parameters as changes in temperature, equipment calibration and numerical aperture of the source stimulate this difference.

4.3 Manual tool looses

By using Matlab® software, from a POF end face image (Figure 51 a) a qualitative view of the end face is generated (Figure 51 b). This qualitative view is based only on normalized intensities, with a resolution of 5.0 Megapixels. The objective of the quantitative images is appreciation.

In POFs, the end face profile is generated with similar regions as those generated in a glass fiber. Figure 51 expose the end face profile in a POF, where the mirror region, which posses the lowest attenuation, is firstly generated. Afterwards a small mist region appears at the end of the cut.

The POF end face regions depends on the type of blade, initial conditions and cleaving process. Thus, Figure 51 can be exposed as a specific case; where after repeating the cleaving procedure with unmodified general parameters, the results were consistents, and the last described behavior is typical in PMMA POF.

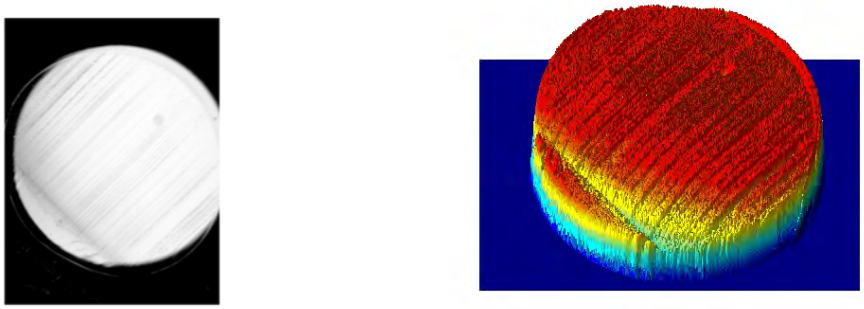

(a) Original image (b) Qualitative view

Figure 51: Image processing of the principal regions of the end face of the POF.

POF jumper attenuation cut by a MOST specialized hand tool
A specialized hand tool, designed for MOST POF, equipped with a circular blade with semi automatic advance was employed (Figure 52) [D2]. The measurement technique was completed according to the standard TIA-526-14-B [D3], and described in Chapter 3 of this work. Following the last standard, Figure 53 shows the implemented laboratory set-up for the attenuation measurement in multimode POF. Cleaves and measurements were performed at an ambient temperature of $\approx$ 25 °C. The length of the fiber in the conducted experiments is 2.25 m.

Figure 52: Specialized stripping and cutting tool for MOST POF.

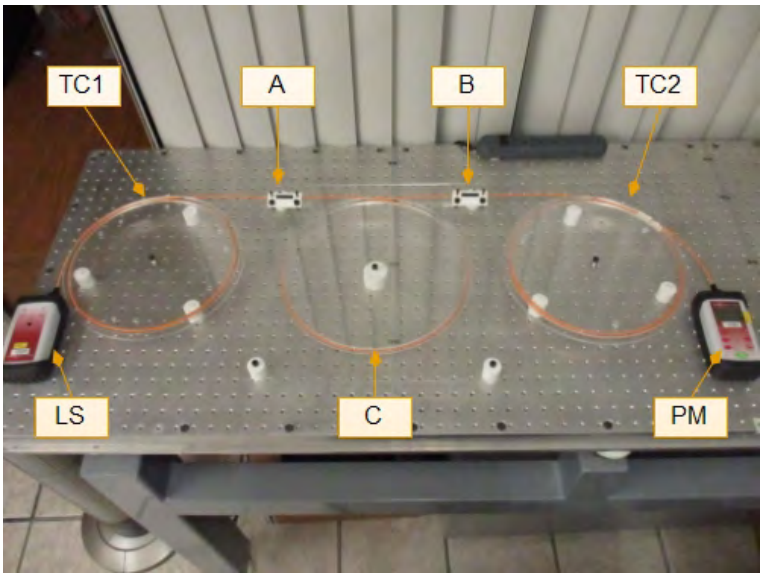

Figure 53: Laboratory set-up for POF attenuation measurement.

Legend			
LS	light source	TC2	receive cord
TC1	launch cord	PM	power meter
C	cable under test	A, B	inline connector

In the conducted experiments, both ends were measured for all cables. The cable value is obtained by the average of both measured end points. The measurement uncertainty was taken from the precision of the measurement equipment, where the half of the minimum digit is used. Therefore, as the power meter precision is limited to one decimal, the error applied is ± 0.05 dB.

Results of cleaving MOST POF with this hand tool are presented in Figure 54.

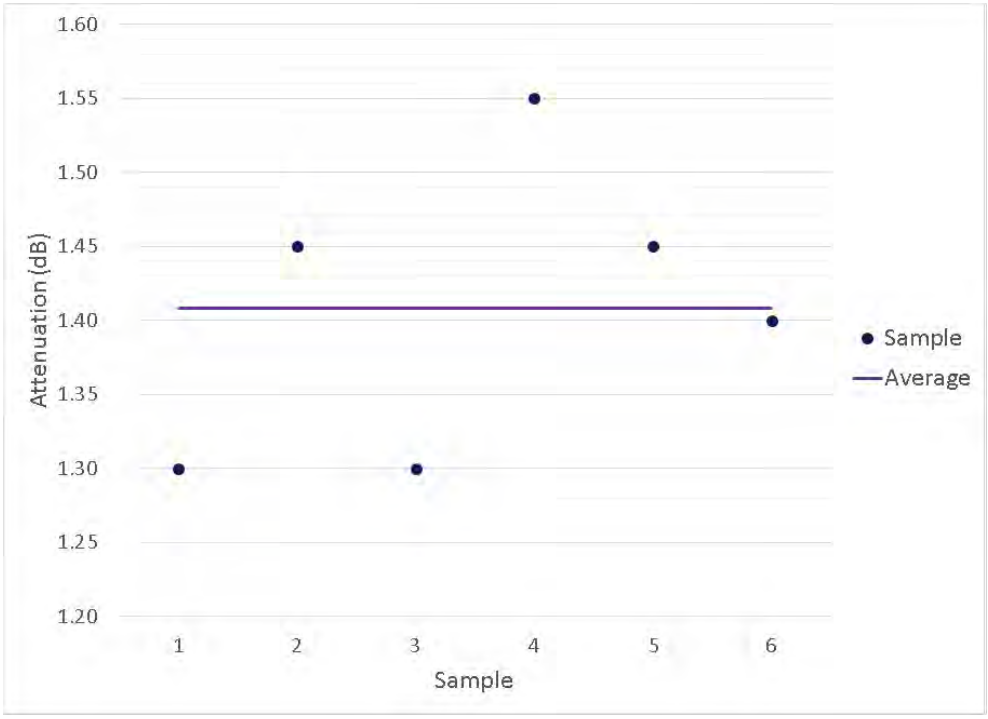

Figure 54: POF cable attenuation by specialized hand tool at 637 nm.

According to the last figure, low loss cleave can be performed while using

only a specialized tool. A primary factor for obtaining low losses is the quality of the blade. Low quality blades will directly increase the attenuation. Also, according with the manufacturer; after 1260 cleaves, the blade degrades and losses arises. Thus, only 630 POF cables can be theoretically manufactured. Another inconvenience is that the operation is not automatic.

4.4 POF jumper semi automatic cleaving device losses

Temperature on the blade

As described in chapter 3 of this work, the semi automatic cleaving device, equipped with an electric heat resistance was employed in order to increase the blade temperature (Figure 55). The blade speed was set to 1 mm/s. By the use of a closed loop temperature controller, the blade temperature was set to *25 ˚C, 90 ˚C, 120 ˚C* and *150 ˚C*. The results of this method are indicated in Figure 56.

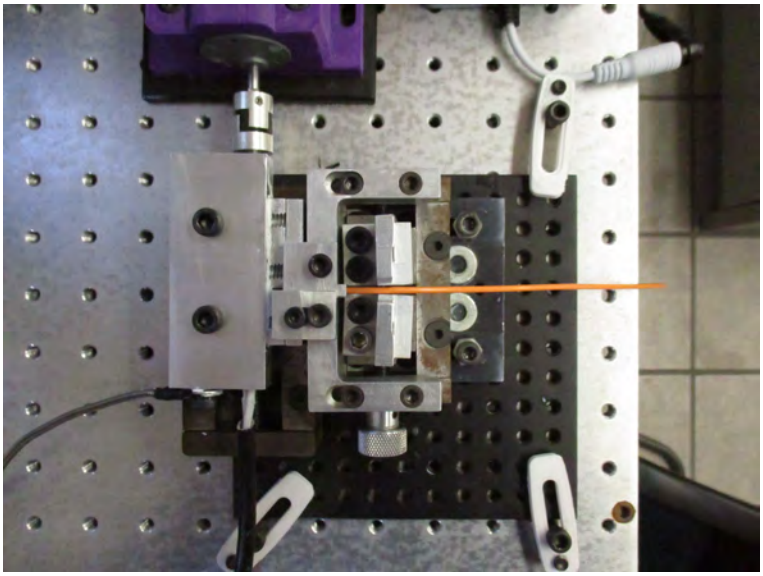

Figure 55: Experimental set-up of the semi automatic cleaving device.

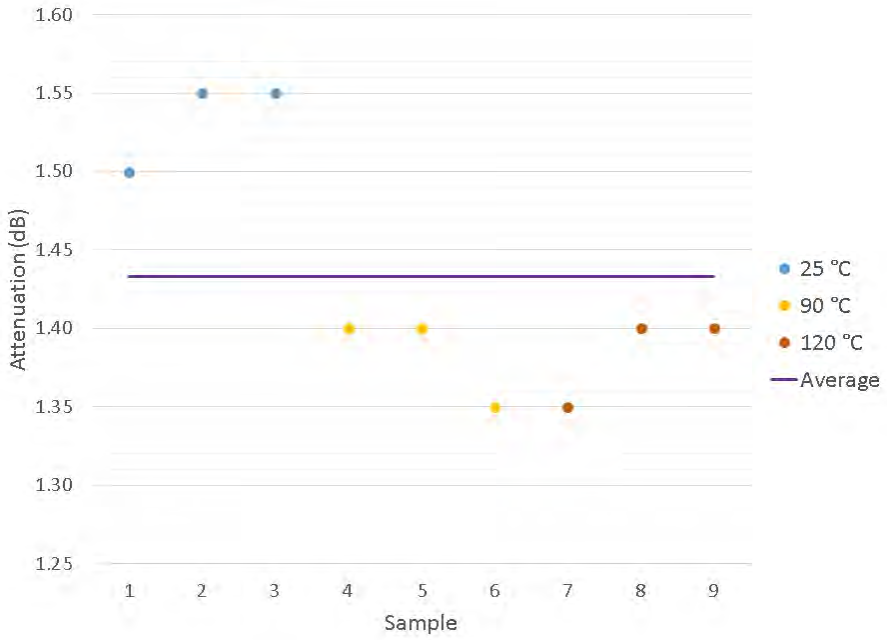

Figure 56: POF jumper attenuation corresponding to the hot blade technique at 637 nm.

As indicated in Figure 56, the range from 90 °C to 120 °C posses similarities with good quality cleaves and low attenuation. Out of this region, the attenuation is increased. With higher temperatures, the material of the inner jacket (PA-12) suffer a fast degradation which contaminates the core. As a result, the 150 °C temperature test was avoided. In the range between ambient temperature and 90 °C, the PMMA core remains in a brittle condition, where the fracture mechanics produces complex results. In the brittle region, crazing cavities are formed after the initial fracture. Thus, a clean end face is not possible to generate [D4].
According to the MOST physical layer [D5], standard MOST fiber have an operational range up to a temperature of 85 °C. Nevertheless, changes in the molecular structure of the PMMA can appear in temperatures as low as 80 °C [D6]. A summary of the transition temperature is available in Chapter 3 of this work.

Reference	Blade Temperature
[D7]	80 °C
[D8]	70 °C - 80 °C
[D9]	50 °C - 80 °C
[D6]	77.5 °C
[D4]	70 °C - 80 °C
[D10]	≈ 110 °C

Table 12: Diverse blade temperatures for hot blade (hot knife) POF cleaving method

As presented in table 12. Several authors differ from the best blade temperature. Nevertheless, the range of 70 °C to 80 °C is common. In particular, the blade temperature must exceed the material transition temperature, without exceeding the temperature at which the melting process of the PMMA core is perceived, this is ≈ 128 °C [D11]. Following the Figure 56, experimental results indicate a low attenuation region founded in the range between 90 °C to 120 °C, which is consistent with the cited literature for the hot blade POF cut method.

Temperature on the fiber
By using the semi automatic cleaving device, hot air heated the fiber guide to *40 °C, 50 °C, 60 °C, 70 °C, 80 °C, 90 °C, 100 °C, 110 °C* and *120 °C* temperatures (Figure 57). An equilibrium time of 90 seconds was used, in order to equilibrate the temperature of the POF. Afterwards, the blade cleaves the POF with a constant speed of 1 mm/s. Results of this method are shown in Figure 58.

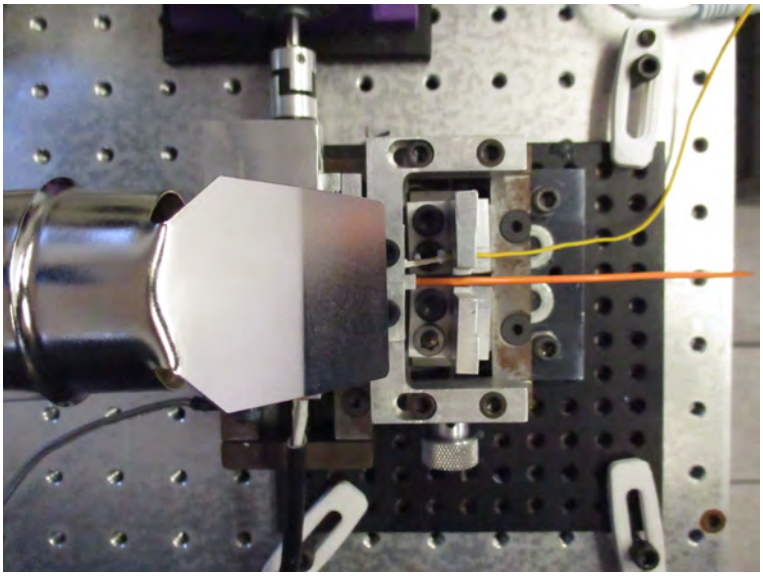

Figure 57: Laboratory set-up for the temperature increase of the POF.

Following the Figure 58, a low attenuation window is located between the temperatures 50 °C and 60 °C. While increasing the temperature further, cable attenuation rises. Above 110 °C, the POF melts before being cleaved. As a result, temperatures beyond 110 °C were avoided.

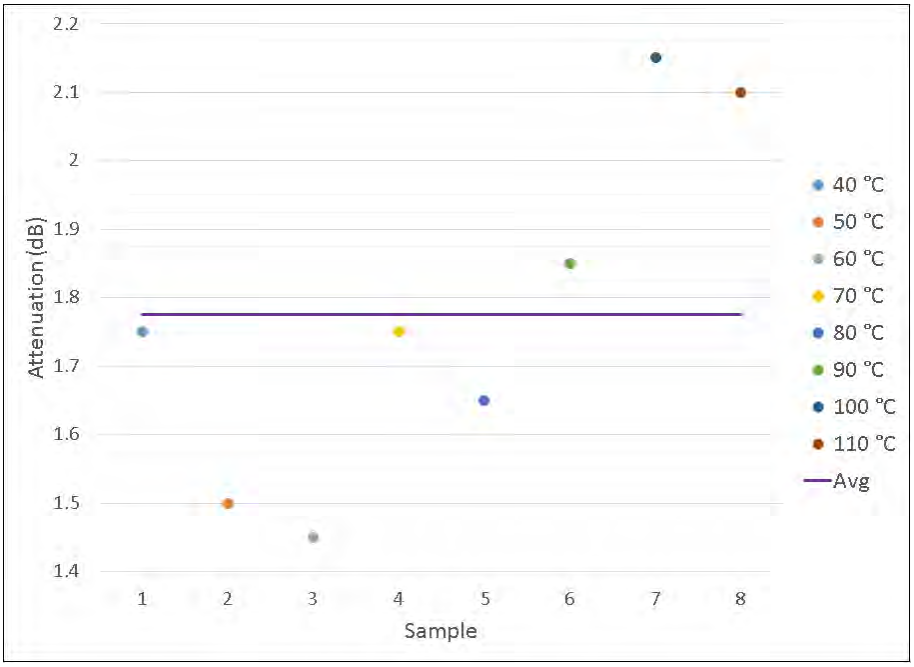

Figure 58: POF cable attenuation for diverse temperatures by incrementing the temperature of the POF.

When increasing both the blade and fiber temperatures at once; it is observed that the major contribution in attenuation is related to the fiber temperature. Thus, blade temperature is irrelevant when combining both blade and fiber temperatures.

4.5 Hot plate termination losses

As previously described in Chapter 3, in this method, a small protrusion of PMMA core is exposed and pressed towards a hot surface. An image of the experimental set-up used is shown in Figure 59. The temperatures conducted in the hot plate termination method were *100 ˚C, 110 ˚C* and *130 ˚C*. Even that the reported literature implies that the exposition time of the end face with the hot surfaces is $\approx$ 10 seconds [D12], or less [D10]; due to the large core of the POF, every end face was pressed against the hot surface for 120 seconds. A slight pressure must be applied when the fiber contacts the hot surface.

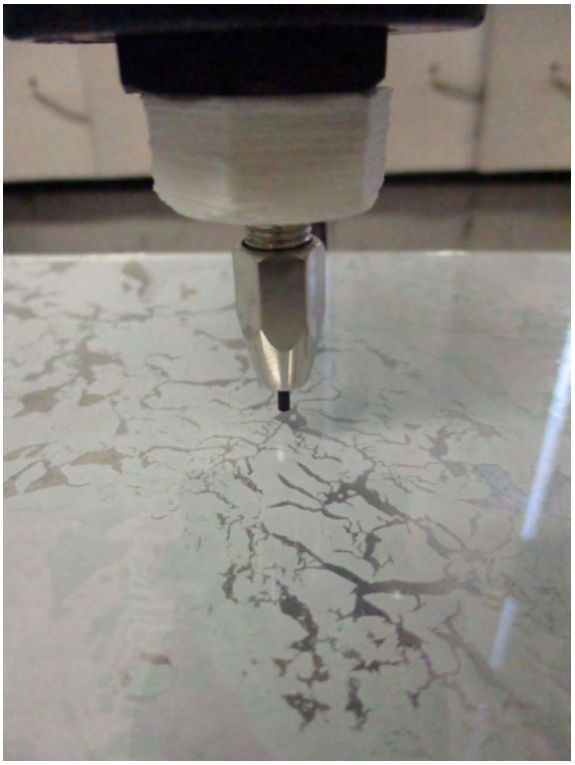

Figure 59: Laboratory set-up for the temperature increase of the POF.

The hot plate termination method posses a large band of attenuation (Figure 60). Best results are obtained in the range of 100 °C to 110 °C. Certain expertise is required in this method as long as the fiber's end face must be with an almost perfect right angle with respect to the mirror surface.

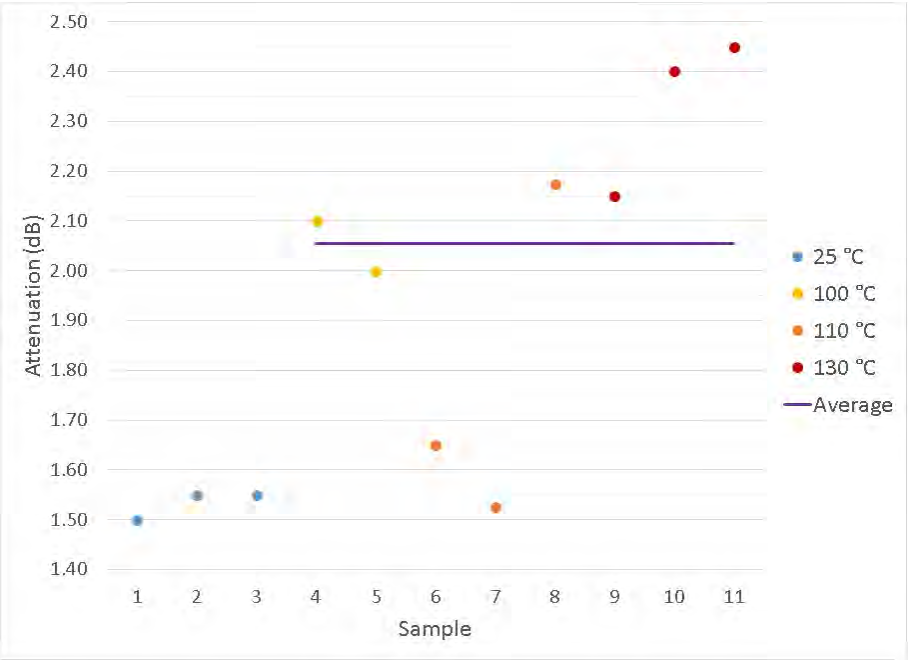

Figure 60: POF jumper attenuation with hot plate at 100 °C, 110 °C and 130 °C. Temperature 25 °C appears as a reference.

Due to the thermal characteristics of the POF cable materials, it is mandatory that only the PMMA core enters in contact with the heated mirror surface. In the case when the PA-12 inner jacket reaches the mirror surface, it will suffer a fast degradation, spreading cladding material into the core.

In comparison with the specialized hand tool, and the semi automatic cleaving device, losses in the hot plate termination method are larger. A probable reason for this effect is that a precise alignment is needed in order that only the core of the POF reaches the hot plate surface. In the case that the inner jacket reaches the heated surface, PA-12 material will contaminate the core, increasing the POF attenuation.

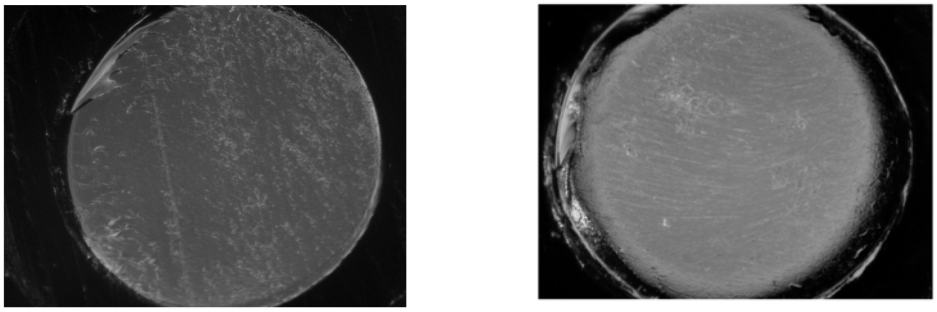

(a) Ambient temperature end face. (b) Hot plate termination at 130 °C.

Figure 61: POF end face modification due to the hot plate termination.

In the Figure 61 is noticed that the hot surface gives shape to the end face of the POF. Due to small particles that could get transferred to the core; a smooth, dust-free surface is ideal for the hot plate termination method.

4.6 Polishing losses

The results of the polishing procedure, previously described in Chapter 3 of this work, are indicated in Figure 62. The first polishing paper, with the biggest grain size (12 μm.), slightly increase the attenuation of the cable when compared with the hand tool cleaving. Also, it flattens the end face of the POF. The consequents polishing papers smooth the end face, until reaching an attenuation of $\approx$ 1 dB. Figure 63 displays the polishing set-up used.

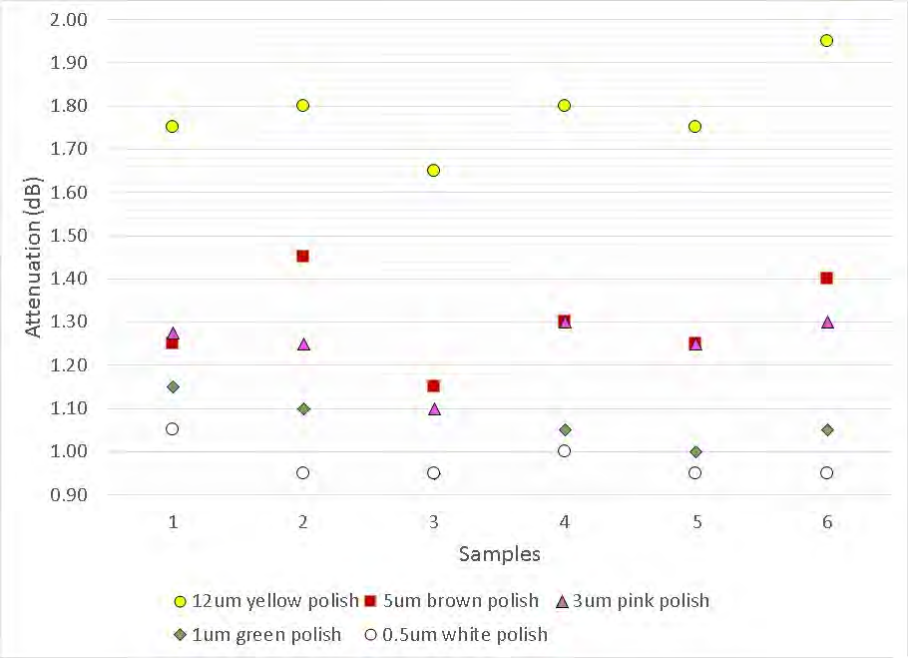

Figure 62: Insertion loss progress of the POF jumpers by the polish method.

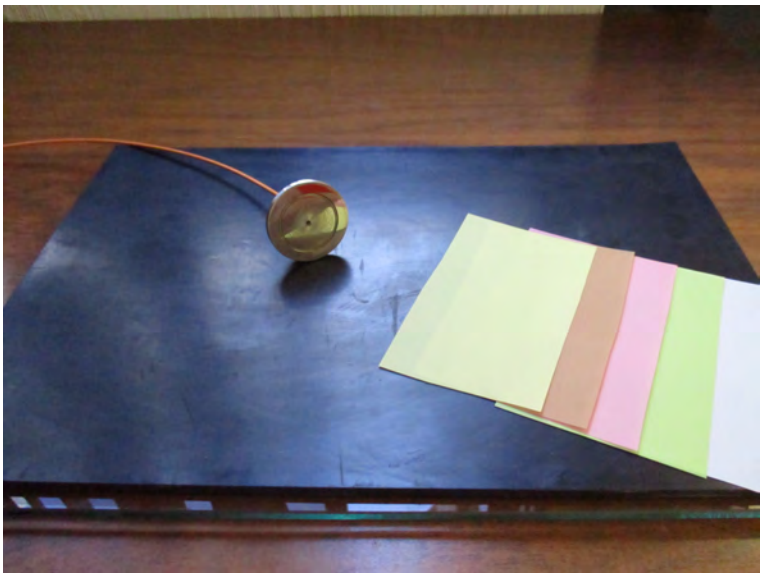

Figure 63: Polish termination laboratory set-up.

As described in Figure 64, reducing the grain size provides not only a decrease in attenuation, but also reduce the variation of the insertion losses. With a smaller grain size, the values of the attenuation are confined into a smaller zone.

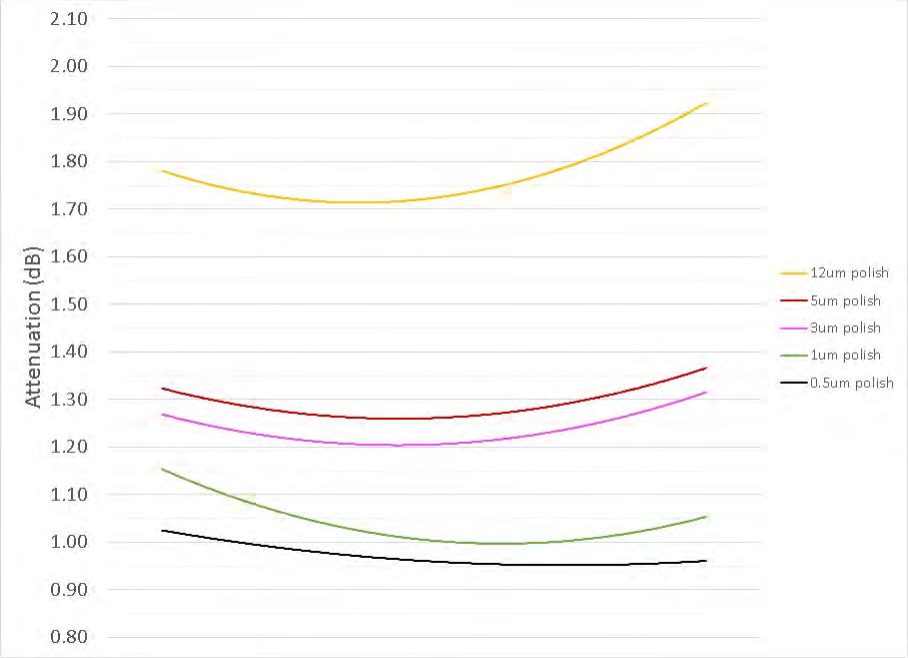

Figure 64: Variation of attenuation according polishing films.

End face POF evolution by the polishing method.
A typical detailed view of the polishing procedure is depicted in Figure 65. As decreasing the grain size of the polishing paper, the smoothness of the end face arises, and the attenuation decreases. Dust or another undesired particles must be avoided while polishing.

Qualitative images offers an appreciative view of the end face profile. In order to obtain a quantitative image of the same, several methods (as shape from shading) have been studied. Nevertheless, due to the high transmittance of the fiber, only interferometric methods can be used. Future work proposes a graphic user interface with a quantitative view of the end face profile in real time.

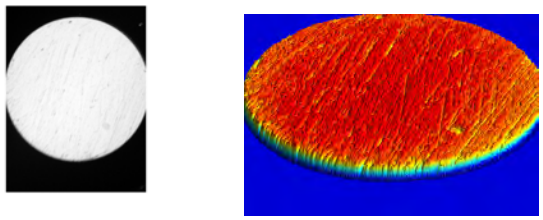

(a) 12 μm polish paper (b) 12 μm polish paper

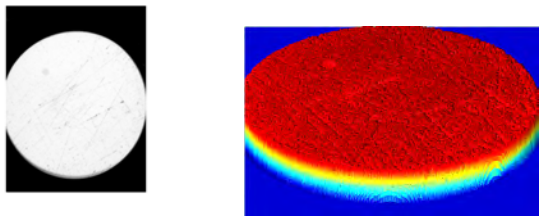

(c) 5 μm polish paper (d) 5 μm polish paper

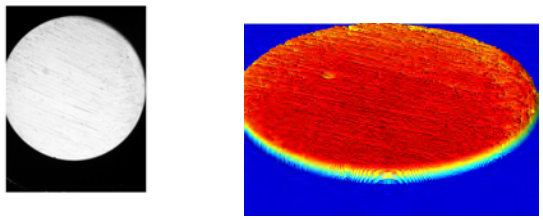

(e) 3 μm polish paper (f) 3 μm polish paper

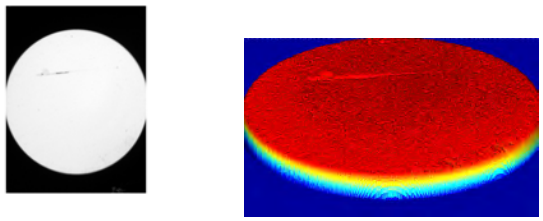

(g) 1 μm polish paper (h) 1 μm polish paper

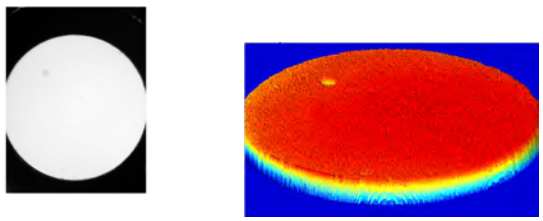

(i) 0.5 μm polish paper (j) 0.5 μm polish paper

Figure 65: Polish end face evolution of POF.

Combination of hot blade cleave and polishing termination methods

The next procedure involves the combination of the hot blade cleave method with the polishing termination method. Firstly, the hot blade cleave method was employed, afterwards POF cables were polished. Results are shown in Figure 66, where it is noticed that the first polishing film (5 μm) flattens the end face of the fiber, and the attenuation increases.

After several conducted tests, it was found that a good approach for low attenuation involves a procedure with two steps: the hot blade cut and the 3 μm. polishing paper. Furthermore, incrementing the number of polishing films below 3 μm. will reduce the fiber attenuation.

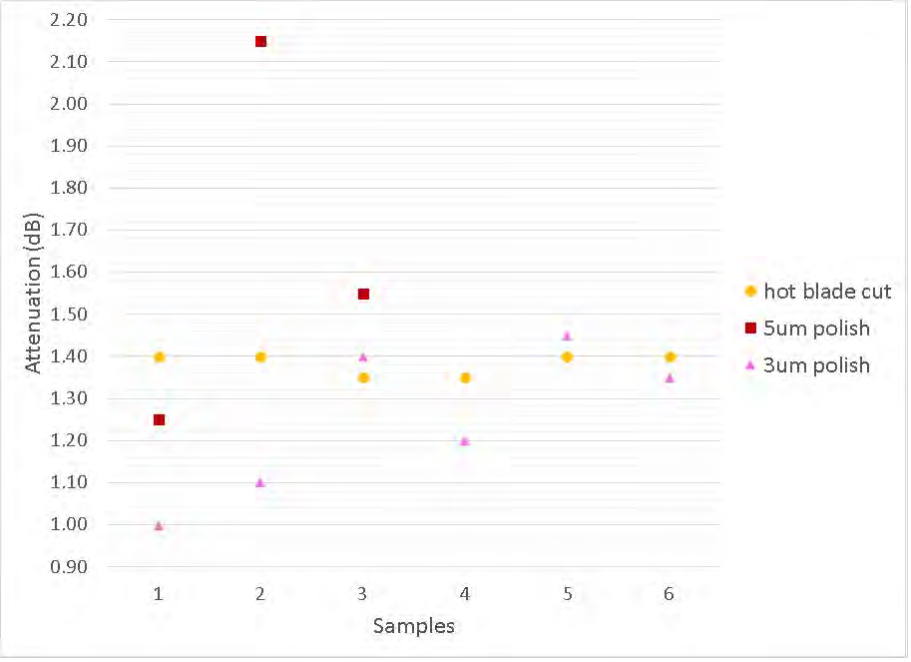

Figure 66: Combination of hot blade cleaving and polish termination attenuation.

Simulations results for termination methods

Using Finite Element Method ANSYS software, a simulation between a hot surface and the POF end face was conducted. Thus, the simulation

supports the Hot plate method. Data of the POF core and inner jacket is described in the Appendix 1 of this work.

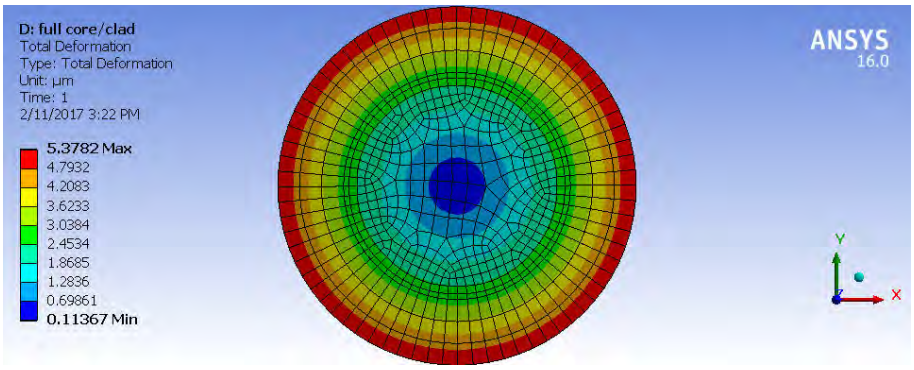

Figure 67: Simulation of the hot plate method. End face view.

Figure 67 represents the mechanical strain due to temperature on the POF end face. When in touch with a hot surface, the PA-12 inner jacket strains faster than the PMMA core. Material values of the core and the inner jacket that were used in simulations, are presented in Appendix 1.

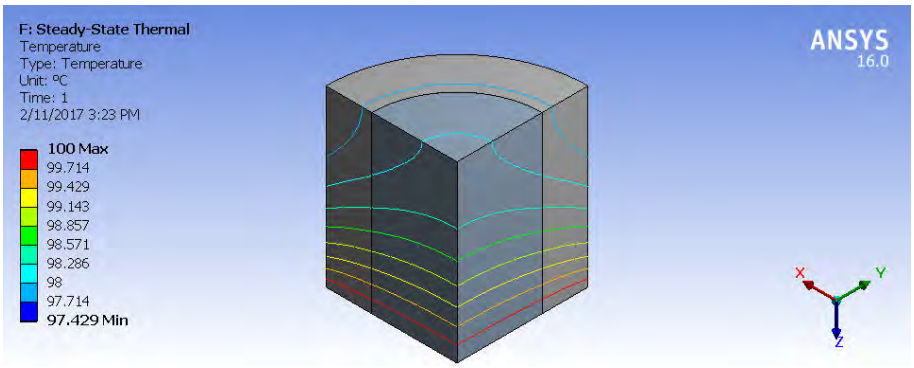

Figure 68: Heat propagation on the core - cladding and inner jacket interface.

In the Figure 68, the POF under test is represented in a quarter view, by cause of two symmetrical axis: the x axis and the y axis [D13]. The ascending lines represent the heat transfer through the PMMA core - cladding and the PA-12 inner jacket, where the heat starts from the base,

thus simulating a contact with the heated surface.

The separation of the lines on the center (PMMA core), indicates that the heat propagation is slower than the PA-12 inner jacket. This result is caused because the thermal coefficient of the inner jacket is larger than the core.

4.7 Comparison of termination methods

A summary of the methods used to decrease the insertion losses are displayed in Figure 69. The largest attenuation is found with the hot plate method at 130 °C. Afterwards, the semi automatic cleaving device posses similar results to the hot plate.

On the middle range, a hand tool with a good quality blade can obtain values close to the semi automatic cut with hot blade method. According to the polishing procedure, the first polishing film will slightly increase the attenuation, then, every polishing film will decrease the attenuation. The lowest attenuation is located with the 0.5 μm polishing film.

A combination of the semi automatic cut with hot blade and polishing film is the most suitable procedure, due that is only required two, or three steps in order to obtain end face losses of ≈ 0.35 dB.

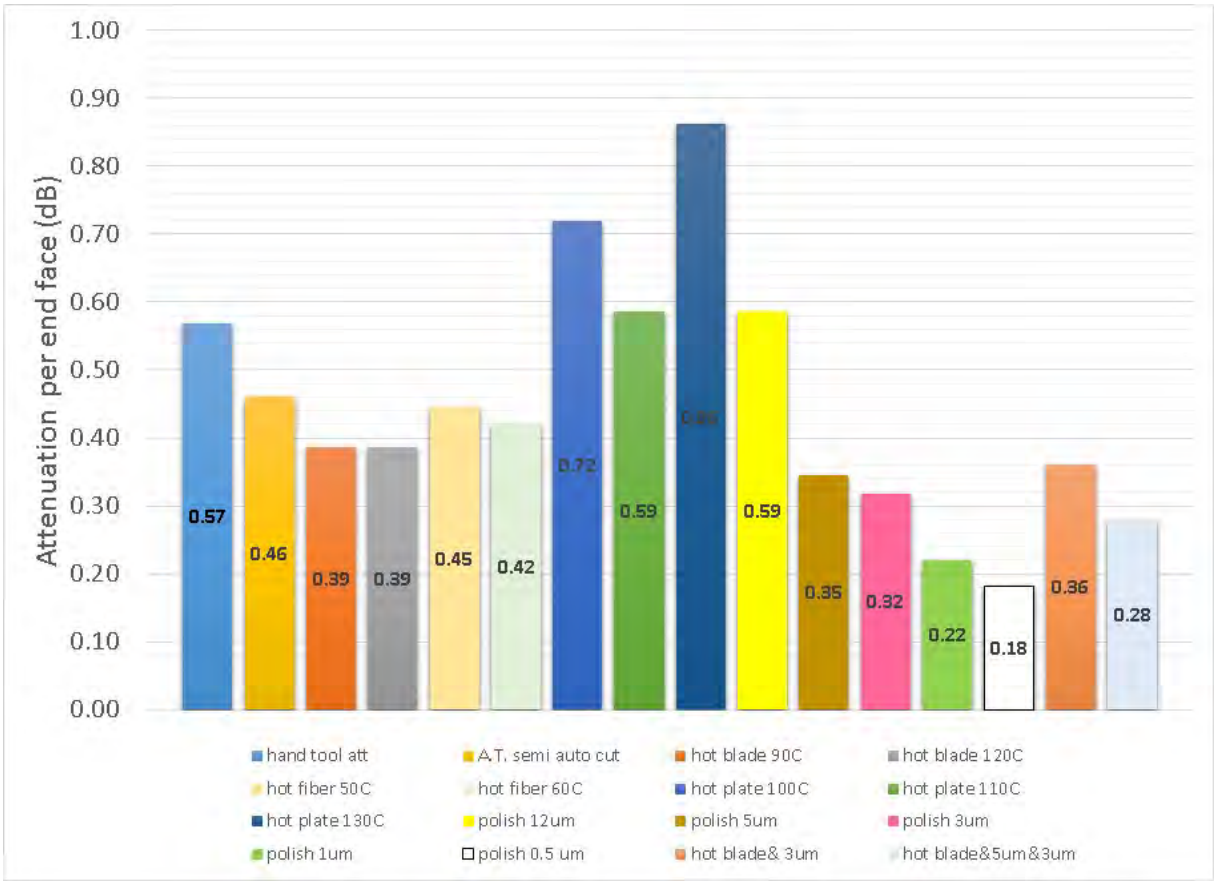

Figure 69: Differences in attenuation per end face of methods described in this work.

In the figure 70, the results obtained are compared wit Reference [D14].

- The semi automatic cleaving device is compared to the reference hot plate.
- The 5 μm polishing film termination and the combination of hot blade with 3 μ polishing film termination are both compared to the value of the reference POF press cut.
- The 1 μm polishing film obtains values slightly above of the reference Fresnel reflection.

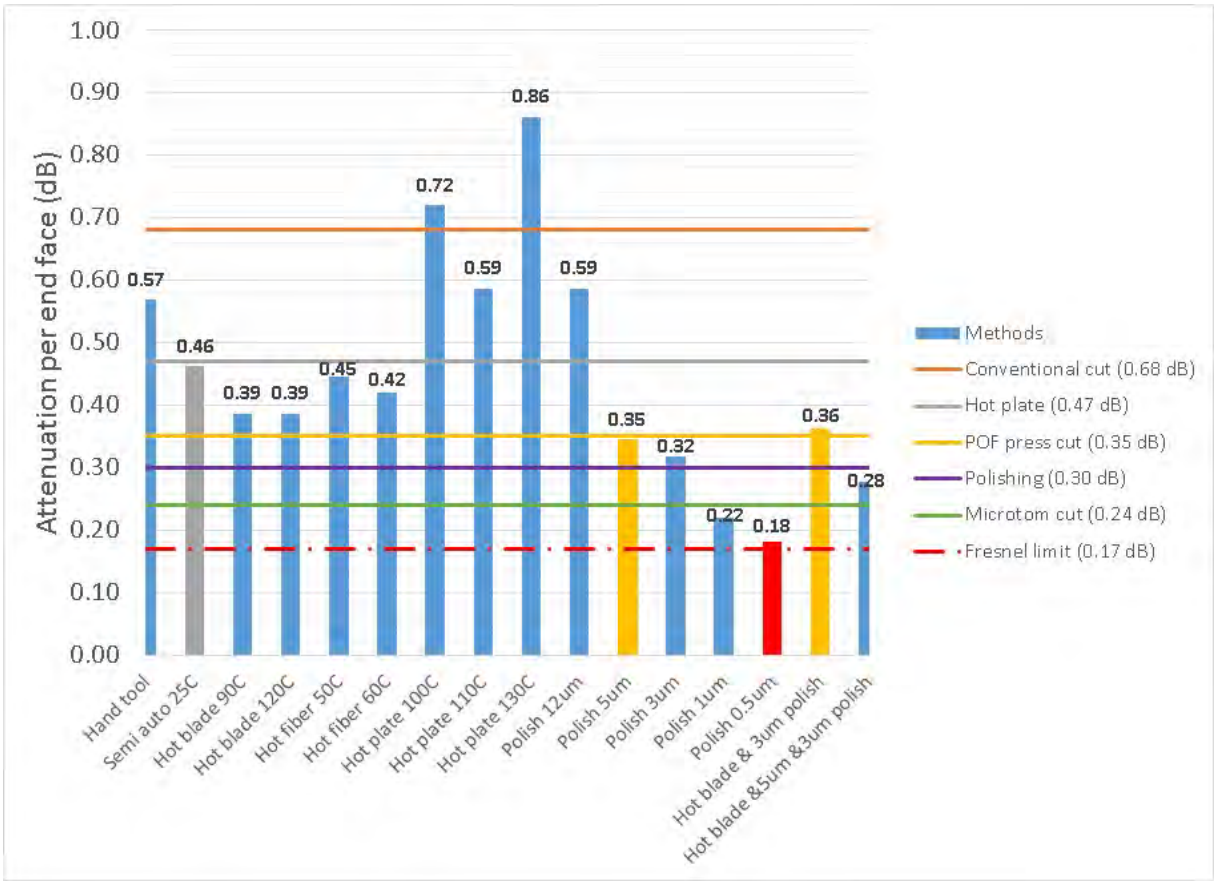

Figure 70: Comparison of results obtained and those reported in reference [D14].

4.8 Chapter 4 conclusions

- The sharp edge of the blade performs the cut of the POF, thicker blades can cleave more POFs than thinner blades. However, thinner blades achieve more clean end faces than a thicker blade, thus producing lower losses.

- In order to obtain the lowest attenuation in the fiber, it is mandatory that the mirror region covers the maximum area of the end surface as possible.

- Due to the difference of the thermal expansion coefficient, when the end face is heated, the PA-12 inner jacket degrades faster than the PMMA core, provoking that the inner jacket spreads and contaminates the core, thus, increasing the attenuation.

- The polishing termination method reduces the variation of the insertion losses. With this method, is possible to achieve losses of ≈ 1 dB.

- With only two steps, a combination of hot blade and a 3 μm polishing film results in the most suitable process for maintaining the average insertion losses equal or below to 1.4 ± 0.1 dB.

4.9

Chapter 4 References

[D1] Mitsubishi. Eska Polymer Optical Fiber. Technical report, Mitsubishi Rayon Co., Ltd., Tokyo, 2016. `http://www.pofeska.com`.

[D2] Rennsteig. Rennsteig Tools, Inc. - Tool for stripping and cutting polymeric optical fibers system MOST, 2016. `http://www.rennsteig.us`.

[D3] Telecommunications industry association. *Optical Power Loss Measurements of Installed Multimode Fiber Cable Plant ; IEC Communications Subsystem Test Procedure- Part 4-1 : Installed cable plant- Multimode attenuation measurement October 2010.* Number October. TIA Telecommunications Industry Association Standard and Engineering Publications, 2010.

[D4] S H Law, M A van Eijkelenborg, G W Barton, C Yan, R Lwin, and J Gan. Cleaved end-face quality of microstructured polymer optical fibres. *Optics Communications*, 265(2):513–520, sep 2006.

[D5] Andreas Grzemba. *MOST: The automotive multimedia network; from MOST25 to MOST150.* Franzis Verlag GmbH, 2011.

[D6] A Stefani, K Nielsen, H K Rasmussen, and O Bang. Cleaving of TOPAS and PMMA microstructured polymer optical fi bers : Core-shift and statistical quality optimization. *OPTICS*, 285(7):1825–1833, 2012.

[D7] O. Abdi, K. C. Wong, T. Hassan, K. J. Peters, and M. J. Kowalsky. Cleaving of solid single mode polymer optical fiber for strain sensor applications. *Optics Communications*, 282(5):856–861, 2009.

[D8] S. Atakaramians, K. Cook, H. Ebendorff-Heidepriem, S. Afshar V., J. Canning, D. Abbott, and T. M. Monro. Cleaving of extremely porous polymer fibers. *IEEE Photonics Journal*, 1(6):286–292, 2009.

[D9] S H Law, J D Harvey, R J Kruhlak, M Song, E Wu, G W Barton, M A van Eijkelenborg, and M C J Large. Cleaving of microstructured polymer optical fibres. *Optics Communications*, 258(2):193–202, feb 2006.

[D10] Van Hove, T Coosemans, B Dhoede, P Van Daele, R Baets, J Van Koetsem, and Framatome Connectors International. Termination olf Small Diameter (125 um) Plastic Optical Fiber for 1x12 Datacommunication. pages 783–789, 1998.

[D11] J. L. Pérez-Castellanos, D. S. Montero, C. Vázquez, J. Zahr-Viñuela, and M. González. Photo-Thermo-Mechanical Behaviour Under Quasi-Static Tensile Conditions of a PMMA-Core Optical Fibre. *Strain*, 52(1):3–13, 2016.

[D12] FiberFin. Hot Plate Termination, 2016. `http://www.fiberfin.com`.

[D13] Katsunari Okamoto, Toshihito Hosaka, and T. Edahiro. Stress analysis of optical fibers by a finite element method. *IEEE Journal of Quantum Electronics*, 17(10):2123–2129, oct 1981.

[D14] Olaf Ziemann, Jürgen Krauser, Peter E. Zamzow, and Werner Daum. *POF Handbook Optical Short Range Transmission Systems*. Springer Berlin Heidelberg, Berlin, Heidelberg, 2008.

5 Conclusions

The improvement of optical communications generates faster, lighter and more reliable data transmission methods. The growth of the automotive industry in the region has required advances in the overall car manufacture. In the automotive networks, optical communications satisfy the increasing demand of high transmission rates at low cost. Within the next years, it is expected that in-vehicle optical communications will be adopted by a larger number of cars. This work focus on the optimization of plastic optical fibers termination processes, which are used in the automotive optical systems.

In comparison with silica fibers, large core plastic optical fibers are improved in handling and costs, but limited in temperature and operational distance. The mechanisms that cause losses in silica fibers are essentially similar to those of plastic optical fibers, but with different magnitude.

The applications of POF include data and non data communication. For data communication, automotive networks have taken in POFs due to its enhanced characteristics over others transmission mediums.

POF supports a favorable cost - benefit relationship for short distance optical links, as those used in the automotive industry. Nevertheless, typical plastic optical fibers are not suitable for high temperatures, the temperature limit of 85 °C reduce the number of applications.

When compared to glass fibers, the geometric tolerances of POF could diminish the costs of tools and equipments. The most common POF cleaving process is the razor blade cleaving, recommendations for this method limits the cleaving for a maximum of two operations.

The objective of a termination method is to obtain a clean cross section of the POF. In this work, terminations methods which involves increments of temperature are exposed. Temperature increase is conducted in order to change the POF core behavior from brittle to ductile. However, other methods which involve decreasing the temperature also produce transitions in the POF materials. Temperatures below -50 °C are needed in the interest of changing the core behavior to essentially inelastic.

When using a razor blade to produce POF cleaving, the sharp edge of the blade performs the cut of the POF. Two perspectives can be stated for the blade thickness: thicker blades can cleave a larger number of POFs than thinner blades, and thinner blades can achieve more clean faces, with lower losses, than a thicker blade. In optical fibers, the lowest attenuation possible is achieved when the mirror region covers the utmost area of the fiber's end face.

Due to the material properties of MOST POFs, the inner jacket material (PA-12) suffer a faster degradation than the core material (PMMA). Furthermore, with and increase of temperature, particles of the inner jacket spreads over the core. This contamination increase importantly the POF attenuation.

An notable advantage of the polishing termination method is the reduction of the variation losses. This method achieve attenuations as low as ≈ 1 dB. In addition, a combination of the hot blade and 3 μm polishing film produce the most suitable process for maintaining the average insertion losses equal or below to 1.4 ± 0.1 dB.

As future work, the results obtained in this work could serve as an early approach to the automation process of the POF cables. Also, a graphic user interface with quantitative view of the end face profile in real time is proposed.

6 Appendix 1. Mechanical Properties of Optical Fibers.

Element	Property	Symbol	Units	Value	Ref.
PMMA	Core diameter	ϕ_{pmma}	μm	980	[Ap1]
	Young's Modulus	E	MPa	3850	[Ap2]
	Yield strength	σ_y	MPa	79.3	[Ap3]
	Tensile strength	σ_t	MPa	85	[Ap2]
	Coeff. of thermal expansion	α	K^{-1}	7 x10^{-5}	[Ap4]
	Density	d	kg m^{-3}	1195	[Ap5]
	Poisson ratio	ν		0.34	[Ap4]
	Thermal conductivity	k	W $m^{-1}K^{-1}$	0.1922	[Ap6]
PA-12	Inner jacket diameter	ϕ_{pa12}	μm	1510	[Ap1]
	Young's Modulus	E	MPa	1450	[Ap7]
	Yield strength	σ_y	MPa	52.5	[Ap7]
	Tensile strength	σ_t	MPa	60.5	[Ap7]
	Coeff. of thermal expansion	α	K^{-1}	11 x10^{-5}	[Ap8]
	Density	d	kg m^{-3}	1.02	[Ap8]
	Poisson ratio	ν		0.35	[Ap9]
	Thermal conductivity	k	W $m^{-1}K^{-1}$	0.23	[Ap8]
SiO_2	Core diameter	ϕ_{Si}	μm	8.2	[Ap10]
	Young's Modulus	E	MPa	70608	[Ap11]
	Yield strength	σ_y	MPa	4903	[Ap11]
	Tensile strength*	σ_t	MPa	4903	[Ap11]
	Coeff. of thermal expansion	α	K^{-1}	1.824 x10^{-9}	[Ap11]
	Density	d	kg m^{-3}	2.2	[Ap11]
	Poisson ratio	ν		0.17	[Ap12]
	Thermal conductivity	k	W $m^{-1}K^{-1}$	1.45576	[Ap13]

*In a SiO_2 stress-strain curve, it is assumed that the rupture strength, yield strength and the tensile strength have the same value. Hence, due to the brittle nature of the fused silica, The tensile strength σ_t, is equated to the yield strength σ_y.

6.1

Appendix 1 References

[Ap1] Mitsubishi Rayon Co. Ltd. GHAN4001-OR1 Data Sheet, 2009.

[Ap2] J. L. Pérez-Castellanos, D. S. Montero, C. Vázquez, J. Zahr-Viñuela, and M. González. Photo-Thermo-Mechanical Behaviour Under Quasi-Static Tensile Conditions of a PMMA-Core Optical Fibre. *Strain*, 52(1):3–13, 2016.

[Ap3] J. L. Pérez-Castellanos, Montero D.S., Vásquez C., and Zahr Viñuelas J. Photo-termo-elastic behaviour of a PMMA-core POF. In *7th International Workshop on Dynamic Behaviour of Materials and its Applications in Industrial Processes*, pages 44–47, Madrid, 2013. Copy Red, S.A.

[Ap4] Manuel Silva-López, Amanda Fender, William N. MacPherson, James S Barton, Julian D.C. Jones, Donghui Zhao, Helen Dobb, David J Webb, Lin Zhang, and Ian Bennion. Strain and temperature sensitivity of a single-mode polymer optical fiber. *Optics Letters*, 30(23):3129, dec 2005.

[Ap5] Kara Peters. Polymer optical fiber sensors—a review. *Smart Materials and Structures*, 20(1):013002, 2011.

[Ap6] M. J. Assael, S. Botsios, K. Gialou, and I. N. Metaxa. Thermal conductivity of polymethyl methacrylate (PMMA) and borosilicate crown glass BK7. *International Journal of Thermophysics*, 26(5):1595–1605, 2005.

[Ap7] Werner Martienssen and Hans Warlimont. *Springer Handbook of Condensed Matter and Materials Data*. Springer Berlin Heidelberg, nov 2005.

[Ap8] Tim A. Osswald, Erwin Baur, Sigrid Brinkmann, Karl Oberbach, and Ernst Schmachtenberg. *International Plastics Handbook*. Carl Hanser Verlag GmbH & Co. KG, München, jun 2006.

[Ap9] MatWeb LLC. PolyOne Gravi-Tech™ GRV-NP-110-W-NAT Polyamide 12 (Nylon 12) Data Sheet, 2016.

[Ap10] Corning Incorporated. Corning ® SMF- 28 ® Ultra Optical Fiber, 2014. http://www.corning.com.

[Ap11] H. Murata. *Handbook of Optical Fibers and Cables*. CRC Press, 1996.

[Ap12] Roger M Wood. Properties, Processing and Applications of Glass and Rare Earth-doped Glasses for Optical Fibres. *Optics & Laser Technology*, 32(1):93, 2000.

[Ap13] Carl L Yaws. *Transport Properties of Chemicals and Hydrocarbons*, volume 1274. Elsevier, 2009.